Ab Initio Calculation of Aqueous Aluminum and Aluminum−Carboxylate Complex Energetics and ^{27}Al NMR Chemical Shifts

J. D. Kubicki,*,† D. Sykes,‡ and S. E. Apitz§

Department of Geosciences, The Pennsylvania State University, University Park, Pennsylvania 16802, Department of Chemistry, 1101 University Ave., University of Wisconsin-Madison, Madison, Wisconsin, and Remediation Research Laboratory, SPAWARSYSCEN D361, 53475 Strothe Rd. Rm. 267D, San Diego, California 92152-6325

Received: August 24, 1998; In Final Form: November 17, 1998

Al^{3+} hydrolysis in aqueous solution was modeled with ab initio calculations. Structural changes surrounding the cation as protons are removed from the initial $Al^{3+}(H_2O)_6$ molecular cluster were predicted. A correlation of the model energy changes and experimental equilibrium constants for these reactions was also found. Calculations of the ^{27}Al NMR chemical shift between the species $Al^{3+}(H_2O)_6$ and $[Al(OH)_4]^-$ were performed to test the feasibility of predicting ^{27}Al NMR chemical shifts in aqueous solution with gas-phase molecular orbital calculations on small clusters. Energetics of Al^{3+}−carboxylic acid complex formation in solution were also calculated using the self-consistent isodensity polarized continuum model (SCIPCM) to account for long-range solvation effects. Comparisons of calculated ^{27}Al NMR chemical shifts in model Al^{3+}−carboxylate complexes to experimentally assigned values were made to test this methodology and previous peak assignments in ^{27}Al NMR spectra of Al^{3+}−carboxylic acid solutions. Results suggest that NMR peaks observed in acidic solutions of carboxylic acids should be re-interpreted in terms of monodentate or protonated bidentate species. Peaks observed as solution pH increases are likely due to formation of aluminum oligomers complexing with ligands and not bidentate complexes with isolated Al^{3+} cations as previously interpreted.

Introduction

Aqueous reactions between aluminum and carboxylic acids are important in environmental chemistry for a number of reasons. Al^{3+}−organic reactions are used in water purification systems to drive coagulation and precipitation of dissolved organic matter and minerals.[1−3] Complexation of Al^{3+} (as well as other metals) by natural organic matter (NOM) has been shown to reduce dramatically the toxicity of the metals compared to an equivalent concentration of free ions.[4−6] Furthermore, Al^{3+}−NOM complexation can affect the transport of organic contaminants that normally partition into NOM.[7,8]

Carboxylic acids, such as those chosen for this study, are thought to represent metal-complexing functional groups in NOM,[9,10] so these simplified complexes should shed light on the nature of more complex Al^{3+}−NOM bonding. In addition, complexation between simple carboxylic acids can increase the solubility and dissolution rates of Al^{3+}-bearing minerals;[11−13] hence, the presence of carboxylic acids can affect the transport of Al^{3+} and other metals within soils, groundwater, and sediments.[14,15] Last, aqueous-phase metal−carboxylate complexation has been assumed to approximate mineral surface−carboxylate bonding.[16] Consequently, models of aqueous Al^{3+}−carboxylate complexation have implications for the mechanisms of chemisorption of NOM on mineral surfaces.[17] In turn, bonding of NOM to mineral surfaces can affect the adsorption of organic contaminants to soils and sediments.[18]

Numerous potentiometric and NMR studies have addressed the problem of aqueous Al^{3+} speciation and Al^{3+}−organic complexation.[19−24] Most of these studies observed broad shoulders forming next to the $Al^{3+}_{(aq)}$ peak at 0 ppm with formation of Al^{3+}−carboxylate complexes. Commonly, these peaks in the 0−20 ppm chemical shift range are assigned to bi- and tridentate complexes whenever there are two or more O-bearing functional groups within the acid molecule. This is true even when the two functional groups are a carboxylate and a phenol group, as in the case of salicylic acid, and the solution is at a fairly low pH.[22] Assignment of these bands to multidentate complexes may be due to the conclusions of Kummert and Stumm[25] that Al^{3+} complexation can lower the pK_a of phenolic groups by 7−10 orders of magnitude and that of Hue et al.[4] that the most stable Al^{3+}−carboxylate complexes are multidentate with five- and six-membered rings formed between the Al^{3+} ion and the organic ligand. However, Kummert and Stumm[25] did propose an equilibrium between monodentate and bidentate complexation that favored the monodentate configurations at low pH (e.g., below pH 3.8 for Al−salicylate).

The purposes of this study are to determine how accurately the ^{27}Al chemical shifts of aqueous phase Al^{3+} and Al^{3+}−organic complexes can be modeled with ab initio, molecular orbital calculations, to test the previous assignments of ^{27}Al chemical shifts with calculations on proposed model species, and to model other possible complexes that may give rise to peaks in the NMR spectra of Al^{3+}−carboxylate solutions. Comparisons of observed and theoretical Al^{3+}−carboxylate vibrational spectra are also made for the Al−salicylate complex to confirm assignments of specific complexes to peaks in the ^{27}Al NMR spectra. Further, energetics of Al^{3+} hydrolysis, Al^{3+}

* To whom correspondence should be addressed. (814) 865-3951, (814) 863-7823 (Fax), kubicki@geosc.psu.edu.
† The Pennsylvania State University.
‡ University of Wisconsin-Madison.
§ Remediation Research Laboratory.

10.1021/jp983462w CCC: $18.00
Published on Web 01/30/1999

dimerization, and Al^{3+}−carboxylate complexation reactions have been calculated and compared to experimental values.

Methods

Standard methods and basis sets of molecular orbital theory as implemented in Gaussian 94[26] were employed to obtain minimum potential energy structures for the molecules and clusters modeled in this study. Calculations were performed with the Hartree−Fock 3-21G** basis set. This basis set was chosen because we have found that it produces reasonably accurate structures with a minimal computational effort to optimize the large number of moderate-sized clusters included in this study.[27] H-bond distances are also reproduced fairly accurately with this basis set.[28] Similar basis sets have been used previously to investigate structures of hydrated metallic cations.[29]

Energy minimizations were performed with the Berny algorithm using the redundant coordinates method of Peng et al.[30] No symmetry constraints were imposed on any of the molecules or clusters. Force constant analyses were performed to ensure that no imaginary frequencies were present and that the structure was in a dynamically stable potential energy minimum. However, we do not claim that any of the structures presented are in the global potential energy minimum. Thermal corrections to the molecular energies were also calculated with the HF/3-21G** basis. Scaling of the zero-point vibrational energies by 0.89 to correct for overestimation of the force constants in the Hartree−Fock and harmonic approximations[31] was included in our estimation of the thermal correction to the molecular energies. Vibrational frequencies were also scaled by 0.89 except for the $C-O_s$ and C−O−Al modes, which were scaled by 0.94. Previous work has shown that this is a better correction factor for this particular mode than the generic 0.89.[32] Scaling of individual modes has been performed by others to obtain more accurate theoretical predictions of vibrational spectra.[33]

Basis set effects on the calculated values of chemical shifts, δ_{iso}, for aqueous Al^{3+} have been investigated previously.[27] Chemical shifts were evaluated based on the NMR standards $Al^{3+}(H_2O)_6$ and $[Al(OH)_4]^-$. Both the basis set used to optimize the molecular structure and that used to calculate the chemical shift were varied. Molecular structure optimizations with HF/3-21G**, HF/6-311+G**, and MP2/6-311+G** calculations were found to give similar δ_{iso}'s for a given basis set used to calculate isotropic chemical shieldings $\{\delta_{iso} = \sigma_{iso}(Al^{3+}) - \sigma_{iso}([Al(OH)_4]^-)\}$. Hence, in this paper, all structures were calculated with the smallest of these basis sets, HF/3-21G**. Of the basis sets used in Sykes et al.[27] to calculate δ_{iso}, the HF/6-31G* basis set gave as consistently good agreement with experiment as any of the larger basis sets. In the present study, similar tests were performed on the monodentate Al^{3+}−oxalate complex with comparable results to those found in Sykes et al.[27] Thus, δ_{iso} values calculated in this paper are based on HF/3-21G** optimized structures and HF/6-31G* σ_{iso}. The effects of increasing the number of explicit H_2O molecules of solvation on the calculated structures and NMR parameters of $[Al^{3+}(H_2O)_6]$, $[Al(OH)_3(H_2O)]$, and $[Al(OH)_4]^-$ were also investigated.

Model aqueous-phase molecular energies were determined with a combination of explicit solvation and self-consistent reaction field techniques.[34,35] Al^{3+} was surrounded by a solvation sphere in each of these Al^{3+} complexes. The self-consistent isodensity polarized continuum model (SCIPCM[26,36,37]) was employed to account for long-range solvation energetics. A dielectric constant of $\epsilon = 78.54$ was used for water at standard temperature and pressure, and a cutoff of 0.001 electrons was chosen for the isodensity surface.[38] Estimates of cavitation energies (ΔE_{cav}) were made following the method of Keith and Frisch[36] with molecular surface areas and volumes calculated with the program AMSOL 5.4 using the PM3-SM3 method[39,40] and HF/3-21G** structures from Gaussian 94.[26] Aqueous-phase deprotonation energies were then estimated from single-point calculations using HF/6-311+G**//HF/3-21G** molecular energies in reactions of the following type

$$Al^{3+}(H_2O)_6 + H_2O{\cdot}8(H_2O) \rightarrow Al(OH)^{2+}(H_2O)_5 + H_3O^+{\cdot}8(H_2O) \quad (1)$$

with each cluster embedded in a polarized continuum.

Results

Effects of Solvation and Basis Set on Structures. Before analyzing the Al^{3+} hydrolysis results, we discuss a test of explicit solvation effects on calculated structures. H_2O molecules were added to the $Al^{3+}(H_2O)_6$, $[Al(OH)_3(H_2O)]{\cdot}2(H_2O)$, and $[Al(OH)_4]^-{\cdot}2(H_2O)$ complexes to form $[Al^{3+}(H_2O)_6]{\cdot}13(H_2O)$, $[Al(OH)_3(H_2O)_2]{\cdot}8(H_2O)$, and $[Al(OH)_4]^-{\cdot}9(H_2O)$, respectively. (Note: In this paper, complexes are enclosed in brackets. Molecular waters bonded to the complex by H-bonds are designated with a "·". Organic ligands are separated by parentheses with their separate charges as superscripts to help clarify the protonation state of the ligand.) Although the addition of this second solvation sphere does not completely account for the long-range ion−dipole and dipole−dipole interactions between the solvent and solute, enlarging the cluster in this manner should indicate whether large structural differences would exist between the original model complexes and aqueous-phase species. Furthermore, longer range solvation effects would be increasingly symmetric about the central Al^{3+} ion and the effects of additional water molecules on the structure and ^{27}Al NMR parameters should begin to cancel out.

Table 1 lists structural parameters for each of the clusters in the Al^{3+} hydrolysis series. Generally, changes in structural parameters upon addition of the second solvation sphere are on the order of 2%. In both the $[Al^{3+}(H_2O)_6]$ and the $[Al^{3+}(H_2O)_6]{\cdot}13(H_2O)$ clusters, $Al^{3+}-OH_2$ distances in $Al^{3+}(H_2O)_6$ are predicted to be close to the experiment range of 1.88−1.90 Å.[41] A second solvation sphere does cause significant structural changes between the $[Al(OH)_3(H_2O)]{\cdot}2(H_2O)$ and $[Al(OH)_3(H_2O)_2]{\cdot}8(H_2O)$ complexes. In the former, Al^{3+} is in irregular tetrahedral coordination; in the latter, Al^{3+} is in trigonal bipyramidal coordination. This is an explicit effect of hydration because energy minimization of the trigonal bipyramidal complex without the extra eight H_2O molecules predicts that the irregular tetrahedron is the more stable structure (i.e., the potential energy of $[Al(OH)_3(H_2O)]{\cdot}(H_2O)$ is less than that of $[Al(OH)_3(H_2O)_2]$). Both of these configurations will be considered when we calculate the ^{27}Al chemical shift of the aqueous complex $Al(OH)_3$.

Table 1 also contains a comparison of structures obtained with HF/3-21G** and MP2/6-311+G** energy minimizations. The MP2/6-311+G** calculations include electron correlation, which should reveal potential problems with the HF/3-21G** structure determinations. Bond lengths are generally 2% longer and HOH bond angles 2% smaller in the MP2/6-311+G** energy-minimized structures when compared to the HF/3-21G** structures. Uncertainties of this level are acceptable for our purposes, especially considering that MP2 calculations tend to overestimate bond lengths.[42] Note that the experimental $Al^{3+}-$

TABLE 1: Structural Parameters of the Al-Hydrolysis Series Complexes with Changes in Explicit Hydration and Basis Set (Bond Lengths in Å and Angles in Degrees)

		method of optimization			
complex	parameter	HF/3-21G**	second solvation sphere	MP2/6-311+G**	SCRF
$Al^{3+}(H_2O)_6$	Al−OH_2	1.912	1.892[a]	1.933	1.925[b]
	O−H	0.953	0.970[a]	0.974	0.981[b]
	HOH	108	111[a]	106	108[b]
$Al(OH)^{2+}(H_2O)_5$	Al−OH	1.661		1.690	
	Al−OH_2	1.948		1.973	
	O−H	0.927		0.958	
$Al(OH)_2^{+}(H_2O)_4$	Al−OH	1.741		1.764	
	Al−OH_2	1.967		2.008	
	O−H	0.934		0.955	
$[Al(OH)_3(H_2O)]\cdot 2(H_2O)$	Al−OH	1.721	1.774[c]	1.750	
	Al−OH_2	1.872	1.962[c]	1.941	
	O−H	0.940	0.942[c]	0.960	
$[Al(OH)_4]^{-}\cdot 2(H_2O)$	Al−OH	1.756	1.759[d]	1.790	
	O−H	0.939	0.945[d]	0.958	
	H···O	1.969	2.060[d]	1.983	

[a] $[Al^{3+}(H_2O)_6]\cdot 13(H_2O)$. [b] Reference 29. [c] $[Al(OH)_3(H_2O)_2]\cdot 8(H_2O)$. [d] $[Al(OH)_4]^{-}\cdot 9(H_2O)$.

OH_2 distances for $Al^{3+}(H_2O)_6$ are 1.88−1.90 Å[41] and that MP2/6-311+G** calculations predict 1.933 Å. Hence, values listed in Table 1 for the HF and MP2 methods will likely bracket the actual values for these complexes.

Water Dissociation. Dissociation of a water molecule is used as a test of the accuracy of our methodology. We have calculated $\Delta E_{(aq)}$ for

$$H_2O\cdot 8(H_2O) \rightarrow 1/2[H_3O^{+}\cdot 8(H_2O) + OH^{-}\cdot 8(H_2O)] \quad (2)$$

and obtained a value of +95 kJ/mol as compared with the experimental ΔH of +56 kJ/mol. Although this is not good quantitative agreement, for the purposes of this paper, reproducing the sign and magnitude of $\Delta E_{(aq)}$ for a reaction will be sufficient to distinguish among possible complexes and configurations.

The discrepancy between experiment and theory mentioned above does not seem to be a function of either the small Hartree−Fock basis set used for structural optimization or the neglect of electron correlation in the energy calculation. To illustrate the former point, the $H_2O\cdot 8(H_2O)$ and $H_3O^{+}\cdot 8(H_2O)$ clusters were reoptimized with a hybrid density functional method using the B3LYP/6-311G* parametrization and basis set.[26,43,44] Both optimizations result in three H bonds of average length 1.60 (HF/3-21G**) and 1.55 Å (B3LYP/6-311G*) from the O atoms of the water molecules to the H atoms of H_3O^{+}. No H bonds were formed to the O atom of the H_3O^{+} molecule, suggesting that H_2O-H_2O H-bonding is stronger than that from H_2O to the O in H_3O^{+}, in agreement with the results of Tuñón et al.[45]

To address the latter point mentioned above, proton solvation energies were calculated with HF/6-311+G**//3-21G**, B3LYP/6-311+G**//3-21G**, and B3LYP/6-311G*//B3LYP/6-311G* methodologies and the SCIPCM.[36] These methods gave solvation energies of −1175, −1166, and −1186 kJ/mol, respectively. Thus, our method of using HF/6-311+G**//3-21G** gives comparable results to those obtained using larger basis sets and density functional theory for energy minimizations. All of these overestimate an average experimental value of −1088 kJ/mol given by Lim et al.[46] by approximately 10%, but our values are close to the estimate of −1153 kJ/mol by Coe et al.[47] It is interesting to note that SCIPCM calculations on H_2O and H_3O^{+} without any explicit waters of hydration using the HF/6-311+G**//3-21G** method result in a ΔH of solvation equal to −1102 kJ/mol, which may be fortuitously close to the average experimental value.[46]

Al^{3+} Hydrolysis. The Al^{3+} hydrolysis series was modeled using the reaction scheme

$$Al^{3+}(H_2O)_6 \rightarrow Al(OH)_n^{3-n}H_2O_{(6-n)} + nH^{+} \quad (3)$$

Energy changes using the SCIPCM and cavitation energy corrections[36] will be designated $\Delta E_{(aq)}$. Structures for the $Al^{3+}(H_2O)_6$ to $[Al(OH)_4]^{-}\cdot 2(H_2O)$ complexes were calculated, and the resulting $E_{(aq)}$ values are listed in Table 2. Two less energetically stable species, *cis*-$Al(OH)_2^{+}(H_2O)_4$ and octahedral $Al(OH)_3(H_2O)_3$,[28b] are also included. The *trans*-$Al(OH)_2^{+}(H_2O)_4$ isomer is 11 kJ/mol lower in potential energy than the *cis*-$Al(OH)_2^{+}(H_2O)_4$ isomer based on our SCIPCM HF/6-311+G** calculations. For $[Al(OH)_3(H_2O)]\cdot 2(H_2O)$ and $Al(OH)_3(H_2O)_3$, the first configuration is 59 kJ/mol lower in potential energy. Hence, we have excluded the *cis*-$Al(OH)_2^{+}(H_2O)_4$ isomer and $[Al(OH)_3(H_2O)_3]$ complex from further calculations and discussion in this study.

Equilibria for Al^{3+} hydrolysis reactions are typically written

$$K_a = [Al(OH)^{3-n}\cdot n(H_2O)][H^{+}]^n/[Al^{3+}(H_2O)_6] \quad (4)$$

Hence, with $\ln(K_a) = -\Delta G/RT$, we solve for ΔH of the reaction

$$RT\ln(K_a) = -\Delta G = -\Delta H + T\Delta S \quad (5)$$

$$RT\ln(K_a) - T\Delta S = -\Delta H \quad (6)$$

A plot of $\ln(K_a)$ from experimental data[48] versus $-\Delta E_{(aq)}$ from our modeling should have a slope equal to RT and an intercept equal to $-T\Delta S$. (The calculated $\Delta E_{(aq)} \approx \Delta H$ except for the PV term included in the enthalpy. PV is small compared to the overall $\Delta E_{(aq)}$ or ΔH terms at ambient pressure.) To determine the $\Delta E_{(aq)}$ of hydrolysis, we have balanced eq 3 with the model reaction

$$H_2O\cdot 8(H_2O)_{(aq)} + H^{+} \rightarrow H_3O^{+}\cdot 8(H_2O)_{(aq)} \quad (7)$$

which has a $\Delta E_{(aq)}$ of −1175 kJ/mol in SCIPCM HF/6-311+G** calculations. Equation 7 actually results in less accurate $\Delta E_{(aq)}$ values than using $H_2O_{(aq)} + H^{+} \rightarrow H_3O^{+}_{(aq)}$. As an example, the experimental ΔH for the first hydrolysis step is +55 kJ/mol[49] compared with our calculated $\Delta E_{(aq)}$ of +8 kJ/mol with eqs 3 and 7 and +79 kJ/mol with a single water molecule to accept the H^{+} charge. It is not clear what compensating error is leading to more accurate energy calcula-

TABLE 2: HF/6-311+G//3-21G** SCIPCM Energies (Hartrees) Corrected by 0.89 ZPE (HF/3-21G**), Thermal Correction - ZPE, and ΔE_{cav}**

cluster	molecular energy	cluster	molecular energy
		Water	
$H_3O^+ \cdot 8(H_2O)$	−684.727 96	$OH^- \cdot 8(H_2O)$	−683.760 79
$H_2O \cdot 8(H_2O)$	−684.280 57		
		Al^{3+} monomers	
$Al^{3+}(H_2O)_6$	−697.967 14	$Al(OH)_3(H_2O)_3$	−696.557 03
$Al(OH)^{2+}(H_2O)_5$	−697.516 45	$[Al(OH)_3(H_2O)] \cdot 2(H_2O)$	−696.579 44
trans-$Al(OH)_2^+(H_2O)_4$	−697.055 96	$[Al(OH)_4]^- \cdot 2(H_2O)$	−696.113 99
cis-$Al(OH)_2^+(H_2O)_4$	−697.051 92		
		Acetate	
$HAc \cdot 8(H_2O)$	−836.060 83	$[(Ac^-)Al^{3+}(H_2O)_4]$	−773.266 11
$Ac^- \cdot 8(H_2O)$	−835.565 31	$[(Ac^-)_2Al^{3+}(H_2O)_4]$	−1000.652 54
$[(Ac^-)Al^{3+}(H_2O)_5]$	−849.315 87		
		Oxalate	
$H_2Ox \cdot 8(H_2O)$	−984.685 82	$[(HOx^-)Al(OH)_2^+(H_2O)_3]$	−996.985 57
$HOx^- \cdot 8(H_2O)$	−984.208 84	$[(H_2Ox)_2Al^{3+}(H_2O)_2]$	−1146.555 47
$Ox^{2-} \cdot 8(H_2O)$	−983.727 43	$[(Ox^{2-})Al^{3+}(H_2O)_4]$	−921.451 11
$[(HOx^-)Al^{3+}(H_2O)_5]$	−997.942 08	$[(Ox^{2-})_2Al^{3+}(H_2O)_2]^-$	−1144.917 97
$[(HOx^-)_2Al^{3+}(H_2O)_4]$	−1297.908 3	$[(Ox^{2-})_3Al^{3+}]$	−1368.372 88
$[(HOx^-)_3Al^{3+}(H_2O)_3]$	−1597.846 76	$[(Ox^{2-})Al(OH)_3]$	−847.621 00
$[(HOx^-)Al(OH)^{2+}(H_2O)_4]$	−997.462 15		
		Catecholate	
$H_2Cat \cdot 4(H_2O)$	−684.509 02	$[(H_2Cat)Al(OH)_2^+(H_2O)_2]$	−925.307 91[c]
$HCat^- \cdot 4(H_2O)$	−684.009 75	$[(Cat^{2-})Al^{3+}(H_2O)_4]$	−925.302 61[c]
		Al dimers	
$[Al_2(OH)_4^{2+}(H_2O)_6]$	−1242.092 58		
		Lactate	
$H_2Lact \cdot 4(H_2O)$	−645.798 14	$[(Lact^{2-})Al^{3+}(H_2O)_4]$	−886.707 02
$HLact^- \cdot 4(H_2O)$	−645.327 72	$[(HLact^-)Al^{3+}(H_2O)_4]$[a]	−887.162 90
$[(HLact^-)Al^{3+}(H_2O)_5]$	−963.197 14	$[(HLact^-)Al^{3+}(H_2O)_4]$[b]	−887.131 88
		Malonate	
$H_2Malon \cdot 4(H_2O)$	−719.576 69	$[(HMalon^-)_2Al^{3+}(H_2O)_4]$	−1375.965 41
$HMalon^- \cdot 4(H_2O)$	−719.100 13	$[(Malon^{2-})Al^{3+}(H_2O)_4]$	−960.451 91
$Malon^{2-} \cdot 4(H_2O)$	−718.602 69	$[(Malon^{2-})_2Al^{3+}(H_2O)_2]$	−1222.951 78
$[(HMalon^-)Al^{3+}(H_2O)_5]$	−1036.962 62	$[(Malon^{2-})_3Al^{3+}]$	−1485.407 32
		Malate	
$H_3Mal \cdot 8(H_2O)$	−1137.595 67	$[(H_2Mal^-)Al^{3+}(H_2O)_4]$	−1074.812 02
$H_2Mal^- \cdot 8(H_2O)$	−1137.118 77	$[(H_2Mal^-)_2Al^{3+}(H_2O)_2]$	−1451.657 73
$HMal^{2-} \cdot 8(H_2O)$	−1136.618 22	$[(HMal^{2-})Al^{3+}(H_2O)_3] \cdot (H_2O)$	−1074.341 38
$Mal^{3-} \cdot 8(H_2O)$	−1136.085 15	$[(Mal^{3-})Al^{3+}(H_2O)_2] \cdot (H_2O)$	−997.840 69
$[(H_2Mal^-)Al^{3+}(H_2O)_5]$	−1150.848 08	$[(Mal^{3-})_2{}^{[4]}Al^{3+}]$	−1297.641 48
$[(H_2Mal^-)_2Al^{3+}(H_2O)_4]$	−1603.725 07		
		Salicylate	
$H_2Sal \cdot 4(H_2O)$	−797.284 88	$Sal^{2-} \cdot 4(H_2O)$	−796.288 09
$HSal^- \cdot 4(H_2O)$	−796.808 79	$[(HSal^-)Al^{3+}(H_2O)_5]$	−1114.678 09

[a] Protonated $Al^{3+}-(OH)-C$ linkage. [b] Bidentate $COOAl^{3+}$. [c] Gas-phase value only.

tions for the case of neglecting the waters of hydration in this case. As mentioned in the Water Dissociation subsection, the $H_2O_{(aq)} + H^+ \rightarrow H_3O^+_{(aq)}$ reaction gives an energy of solvation approximately 85 kJ/mol less than the $H_2O \cdot 8(H_2O)_{(aq)} + H^+ \rightarrow H_3O^+ \cdot 8(H_2O)_{(aq)}$ value, so this discrepancy may be explained by the differences in the calculation of $H^+ \rightarrow H_3O^+ \cdot 8(H_2O)_{(aq)}$ rather than $Al^{3+}(H_2O)_6 \rightarrow Al(OH)_n^{3-n}H_2O_{(6-n)} + nH^+$ (eq 3). This problem is also exposed by comparison of our Al^{3+} hydration energies to Born model results and experimental data. $\Delta H_{abs}(Al^{3+})$ in our study is −4690 kJ/mol compared with Born model results of −4677 to −4699 kJ/mol.[50] However, agreement of our calculated $\Delta H_{rel}(Al^{3+})$ value with experiment[52] is not as good (−1168 versus −1387 kJ/mol, respectively), which is attributable to the error in $\Delta H_{abs}(H^+)$.

Figure 1 shows the correlation between $\ln(K_a)$ and $-\Delta E_{(aq)}$ for our SCIPCM HF/6-311+G**//HF/3-21G** calculations with the activation energy correction. The correlation coefficient is good ($R^2 = 0.989$), indicating that the calculations are modeling the essential aspects of the hydrolysis reactions in solution. A slope of 4.0 ± 0.3 kJ/mol/$\ln(K_a)$ translates into a theoretical temperature of 475 ± 36 K, approximately 175 K from the ideal 298 K. The y intercept of +43 ± 11 kJ/mol predicts ΔS of hydrolysis = −92 ± 23 J/(mol K), comparable to the experimental value of −80 J/(mol K) for the reaction $H_2O_{(aq)} \rightarrow (OH)^-_{(aq)} + H^+_{(aq)}$. Although there is room for improvement in the accuracy of the model energetics, we contend that the overall correlation of thermodynamic parameters strongly suggests that the models closely mimic aqueous Al^{3+} hydrolysis.

Al^{3+}−Carboxylate Complexation Energetics. Calculation of complexation energies can be used to predict which species may be more energetically stable. Thermodynamic constraints can then be used in conjunction with the theoretical NMR chemical shifts to determine which species are likely to be present in solution and which give rise to particular NMR peaks. Table 2 lists model aqueous-phase molecular energies, $E_{(aq)}$, for various complexes in this study. Although the basis set used in these energy calculations is fairly large, neglect of structural relaxation within the model solvent could be a significant source

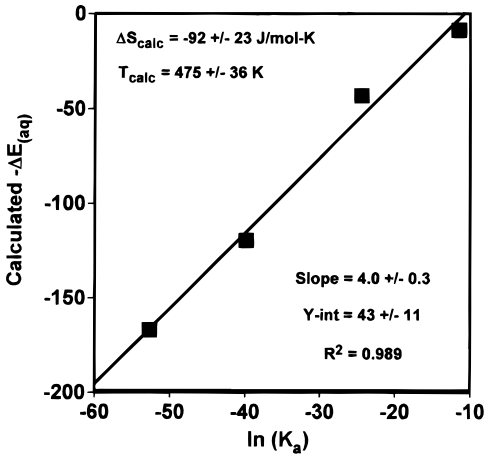

Figure 1. Calculated energy changes correlated with experimental ln(K_a) values from Wesolowski and Palmer[48] for Al^{3+} hydrolysis.

of error in our estimates of aqueous molecular energies. Hence, the absolute values of $E_{(aq)}$ are probably not extremely accurate. However, structural relaxation within SCRF calculations does not change bond lengths and angles by more than a few percent in the case of $Al^{3+}(H_2O)_6$ (Table 1), so we do not expect dramatic changes in $\Delta E_{(aq)}$ upon structural relaxation within a polarized continuum. Furthermore, this effect is neglected for all the complexes. Consequently, *relative* $\Delta E_{(aq)}$ calculations between complexes should be accurate on a semiquantitative level. We will test this conclusion where experimental ΔH data is available.

Acetate and Lactate. Two main conclusions can be drawn regarding the complexation of Al^{3+} with acetate (Ac^-) and lactate ($HLact^-$) from the results in Table 2. (Note: In this paper, organic acids are referred to with the number of ionizable protons present listed first. The overall charge on the ligand is listed as a superscript. For example, lactic acid has two ionizable protons and is designated H_2Lact. After removal of the carboxyl proton, the species is $HLact^-$, and after the second proton is removed it is $Lact^{2-}$.) First, reactions in which acetate anion replaces an H_2O group have negative ΔE's, whereas reactions in which acetate anion replaces an $(OH)^-$ group have positive ΔE's. For example,

$$Ac^-\cdot 8(H_2O) + Al^{3+}(H_2O)_6 \rightarrow [(Ac^-)Al^{3+}(H_2O)_5] + H_2O\cdot 8(H_2O), \quad \Delta E = -168 \text{ kJ/mol} \quad (8a)$$

$$HAc\cdot 8(H_2O) + Al^{3+}(H_2O)_6 \rightarrow [(Ac^-)Al^{3+}(H_2O)_5] + H_3O^+\cdot 8(H_2O), \quad \Delta E = -42 \text{ kJ/mol} \quad (8b)$$

and

$$Ac^-\cdot 8(H_2O) + Al(OH)^{2+}(H_2O)_5 \rightarrow [(Ac^-)Al^{3+}(H_2O)_5] + OH^-\cdot 8(H_2O), \quad \Delta E = +13 \text{ kJ/mol} \quad (9a)$$

$$2[Ac^-\cdot 8(H_2O)] + Al(OH)_2^+(H_2O)_4 \rightarrow [(Ac^-)_2Al^{3+}(H_2O)_4] + 2[OH^-\cdot 8(H_2O)], \quad \Delta E = +33 \text{ kJ/mol} \quad (9b)$$

The latter values are similar to the $\Delta H = +17 \pm 6$ and $+30 \pm 30$ kJ/mol measured for Al^{3+}−acetate complexation at 25 °C;[51] however, the experimental values apply to replacement of H_2O rather than OH^-. For Ac^- replacing OH^-, the ΔH was found to be 0 ± 1 kJ/mol,[51] suggesting that Ac^- binds as strongly to Al^{3+} as OH^-. The reason for this discrepancy between our model and the experimental results is not clear. Although it is possible that these calculations are in error, there are two arguments against this being the case. One is that the calculated Al^{3+} hydrolysis energetics are similar to measured ΔH values. The other reason is that the cation−anion bond between Al^{3+} and acetate should be stronger than the cation−dipole bond between Al^{3+} and H_2O (i.e., the energy change for substituting acetate for a water molecule should be negative as calculated). Loss of Coulombic energy could offset the energy gained by pairing the two charged species, but at infinite dilution, the Coulombic term between the Al^{3+} cation and the acetate anion should be negligible. Perhaps the experimental data could be re-interpreted in terms of different reactions based on the model results reported here.

The second conclusion that may be drawn from Table 2 is that the formation of bidentate species are less energetically stable than monodentate species. For example,

$$Ac^-\cdot 8(H_2O) + Al^{3+}(H_2O)_6 \rightarrow [(Ac^-)Al^{3+}(H_2O)_4] + 10(H_2O), \quad \Delta E = -119 \text{ kJ/mol} \quad (10a)$$

or

$$Ac^-\cdot 8(H_2O) + Al(OH)_2^+(H_2O)_4 + 8(H_2O) \rightarrow [(Ac^-)Al^{3+}(H_2O)_4] + 2[(OH)^-\cdot 8(H_2O)], \quad \Delta E = +218 \text{ kJ/mol} \quad (10b)$$

compared to −168 or +13 kJ/mol for the monodentate reactions above (eqs 8a and 9a). Monodentate configurations are consistent with most interpretations of aqueous Al^{3+}−acetate and Al^{3+}−lactate complexes.[22]

Lactate can possibly form bidentate complexes with Al^{3+} via the carboxylate and hydroxyl oxygens. Comparison of the calculated energies for the bidentate reaction versus monodentate reaction shows that the two have similar model enthalpies.

$$HLact^-\cdot 4(H_2O) + Al^{3+}(H_2O)_6 \rightarrow [(HLact^-)Al^{3+}(H_2O)_4] + 6(H_2O), \quad \Delta E = -145 \text{ kJ/mol} \quad (11a)$$

$$HLact^-\cdot 4(H_2O) + Al^{3+}(H_2O)_6 \rightarrow [(HLact^-)Al^{3+}(H_2O)_5] + 5(H_2O), \quad \Delta E = -152 \text{ kJ/mol} \quad (11b)$$

The bidentate reaction should have a more positive entropy change due to the release of two H_2O molecules from the Al^{3+} cation, and hence, the protonated bidentate species could be favored by the overall ΔG of reaction. Deprotonation of $[(HLact^-)Al^{3+}(H_2O)_4]$ to form $[(Lact^{2-})Al^{3+}(H_2O)_4]$ results in a calculated $\Delta E_{(aq)}$ of +22 kJ/mol. Compared to the calculated $\Delta E_{(aq)}$ value for $Al(OH)^{2+}(H_2O)_5 \rightarrow Al(OH)_2^+(H_2O)_4$ of +34 kJ/mol, the protonated bidentate species $[(HLact^-)Al^{3+}(H_2O)_4]$ is more likely to form than $Al(OH)_2^+(H_2O)_4$.

The deprotonated bidentate species $[(Lact^{2-})Al^{3+}(H_2O)_4]$ also has a negative ΔE_{aq} (eq 12a), but it is less than that of the protonated counterpart $[(HLact^-)Al^{3+}(H_2O)_4]$ (eq 11a).

$$HLact^-\cdot 4(H_2O) + Al^{3+}(H_2O)_6 + 3(H_2O) \rightarrow [(Lact^{2-})Al^{3+}(H_2O)_4] + (H_3O)^+\cdot 8(H_2O), \quad \Delta E = -123 \text{ kJ/mol} \quad (12a)$$

$$HLact^{-}\cdot 4(H_2O) + Al(OH)^{2+}(H_2O)_5 \rightarrow [(Lact^{2-})Al^{3+}(H_2O)_4] + 6(H_2O), \quad \Delta E = -130 \text{ kJ/mol} \quad (12b)$$

Thus, lactate could form bidentate complexes with Al^{3+} and be a weaker complex former than acetate[4] because these $\Delta E_{(aq)}$ complexation values are lower than the potential value predicted in eq 8a for acetate replacing H_2O. This conclusion contradicts a common assumption that $Al^{3+}-$carboxylate complexes with larger binding constants have bidentate or multidentate structures.

Oxalate, Malonate, and Malate. As in the case for $Al^{3+}-$acetate complexes, the model $Al^{3+}-$oxalate, $Al^{3+}-$malonate, and $Al^{3+}-$malate complexes showed strong negative $\Delta E_{(aq)}$ for replacement of H_2O groups by the organic anion and positive changes for replacement of OH^- groups. Although bidentate replacement of water molecules by oxalate and malate is more strongly favored, monodentate speciation by the singly deprotonated species is also exothermic. For example,

$$Ox^{2-}\cdot 8(H_2O) + Al^{3+}(H_2O)_6 \rightarrow [(Ox^{2-})Al^{3+}(H_2O)_4] + 10(H_2O), \quad \Delta E = -177 \text{ kJ/mol} \quad (13a)$$

$$HOx^{-}\cdot 8(H_2O) + Al^{3+}(H_2O)_6 \rightarrow [(HOx^{-})Al^{3+}(H_2O)_5] + H_2O\cdot 8(H_2O), \quad \Delta E = -123 \text{ kJ/mol} \quad (13b)$$

and

$$HOx^{-}\cdot 8(H_2O) + Al^{3+}(H_2O)_6 \rightarrow [(Ox^{2-})Al^{3+}(H_2O)_4] + H_3O^{+}\cdot 8(H_2O) + H_2O, \quad \Delta E = -88 \text{ kJ/mol} \quad (13c)$$

Thus, under pH conditions where oxalic and malic acids are not dissociated (i.e., $\leq$ pH 3), $Al^{3+}-$oxalate and $Al^{3+}-$malate monodentate complexation could be energetically favored. The above result is significant because many NMR studies of Al complexation in aqueous solution are performed under acidic conditions to avoid oligomerization and precipitation of Al.

We also note that monodentate replacement of H_2O by Ox^{2-} does not occur in our model calculations. In the monodentate species, $[(Ox^{2-})Al^{3+}(H_2O)_5]$ and $[(Ox^{2-})Al(OH)^{2+}(H_2O)_4]$, H^+ transfers occur from one of the remaining H_2O groups to the Ox^{2-} ligand during energy minimization thereby forming the species $[(HOx^{-})Al(OH)^{2+}(H_2O)_4]$ and $[(HOx^{-})Al(OH)_2^{+}(H_2O)_3]$, respectively. Removal of the proton bonded to the oxalate ligand in $[(HOx^{-})Al(OH)_2^{+}(H_2O)_3]$ causes Al^{3+} to undergo a coordination change to a pentacoordinate species with the oxalate becoming a bidentate ligand (i.e., $[(Ox^{2-})Al(OH)_2^{+}(H_2O)]\cdot 2(H_2O)$ with one water bonded to Al^{3+} and the other two water molecules hydrating the complex).

Experimental enthalpies are available for $Al^{3+}-$malonate and $Al^{3+}-$dimalonate complexes. Ridley et al.[53] report ΔH values of $+19 \pm 5$ and $+29 \pm 10$ kJ/mol, respectively, for these two complexes. Our calculated values for replacement of H_2O molecules by malonate predict a large negative energy change, inconsistent with these measured values. However, if the reactions are written in terms of anion exchange of monodentate malonate for OH^-, then the model values of $+39$ and $+49$ kJ/mol for these complexation reactions are reasonably close to experiment.

Protonated bidentate configurations were modeled for $Al^{3+}-$malate complexes. The potential energy difference between the monodentate species $[(H_2Mal^{-})Al^{3+}(H_2O)_5]$ and the protonated bidentate species $[(H_2Mal^{-})Al^{3+}(H_2O)_4] + H_2O$ is only $+13$ kJ/mol (Table 2). Although a complex with an $Al^{3+}-(OH)-C$ linkage may at first seem to be an unstable configuration, the calculated energy change for deprotonation of the bridging hydroxyl group,

$$[(H_2Mal^{-})Al^{3+}(H_2O)_4] + H_2O\cdot 8(H_2O) \rightarrow [(HMal^{2-})Al^{3+}(H_2O)_4] + H_3O^{+}\cdot 8(H_2O) \quad (14)$$

is $+61$ kJ/mol, which is greater than that calculated for removing two protons from $Al^{3+}(H_2O)_6$ to form $Al(OH)_2^{+}(H_2O)_4$. Thus, the proton in the $Al^{3+}-(OH)-C$ linkage is less acidic than those in $Al^{3+}(H_2O)_6$ and $Al(OH)^{2+}(H_2O)_5$, so $[(H_2Mal^{-})Al^{3+}(H_2O)_4]$ could exist at pH's higher than the first two pK_a's of $Al^{3+}_{(aq)}$ (i.e., pH 5).

Catecholate and Salicylate. We were unable to calculate aqueous-phase energies for most of the $Al^{3+}-$catecholate and $Al^{3+}-$salicylate species with HF/6-311+G** SCIPCM calculations even though stable structures were found with the gas-phase energy minimizations. Multiple attempts to find converged solutions to the self-consistent field electron densities resulted in no electron configurations within the convergence limits. Calculation of the $Al^{3+}-$catecholate and $Al^{3+}-$salicylate complexation energies is not possible without the aqueous-phase energies for these species. A comparison can be made, however, between two $Al^{3+}-$catecholate species with the same charge. These two species, $[(Cat^{2-})Al^{3+}(H_2O)_4]$ and $[(H_2Cat)Al(OH)_2^{+}(H_2O)_2]$, should have similar solvation energies because they have the same composition and charge (they differ by the placement of protons either on $Al^{3+}-(OH_2)$ groups or $Al^{3+}-(OH)-C$ linkages). Hence, comparison of the gas-phase energies for these two complexes could be an indicator of stability in solution as well. The protonated bridging bidentate $[(H_2Cat)Al(OH)_2^{+}(H_2O)_2]$ complex was predicted to be more stable in the gas phase by -14 kJ/mol (Table 2). This result is significant because it is generally assumed that $Al^{3+}-$catecholate complexes form via $Al^{3+}-O-C$ linkages at pHs above 3; but, if our results are correct, then $Al^{3+}-OH_2$ groups may deprotonate before the $Al^{3+}-(OH)-C$ linkages formed at pH's less than 3. Potentiometric data may not be able to discriminate between two species of the same charge varying only by the location of the protons.

One $Al^{3+}-$salicylate complex, the monodentate species $[(HSal^{-})Al^{3+}(H_2O)_5]$, did produce a converged self-consistent electron density and an aqueous energy. The complexation energies for the reactions

$$[Al^{3+}(H_2O)_6] + HSal^{-}\cdot 4(H_2O) \rightarrow [(HSal^{-})Al^{3+}(H_2O)_5] + 5(H_2O) \quad (15a)$$

and

$$[Al(OH)^{2+}(H_2O)_5] + HSal^{-}\cdot 4(H_2O) + 4(H_2O) \rightarrow [(HSal^{-})Al^{3+}(H_2O)_5] + OH^{-}\cdot 8(H_2O) \quad (15b)$$

were calculated to be -142 and $+21$ kJ/mol, respectively. Both of these values are similar to values obtained for the nonbenzoic carboxylic acids discussed above, suggesting that the aromatic ring does not play a large role in the determination of Al−carboxylate complex formation, at least for monodentate species.

NMR Calculations. A detailed discussion of calculations on the δ_{iso} for ^{27}Al between the standards $Al^{3+}(H_2O)_6$ and $[Al(OH)_4]^-$ can be found in Sykes et al.[27] Although the error in $\delta_{iso}(^{27}Al)$ for $[Al(OH)_4]^-$ in Table 3 is only 2 ppm using the

TABLE 3: Comparison of HF/6-31G*//3-21G Calculated ^{27}Al Chemical Shifts ($\delta(^{27}Al)_{Theory}$) and Previous Assignments Based on Observed Peaks in Aqueous Solutions ($\delta(^{27}Al)_{expt}$)**

molecule	$\delta(^{27}Al)_{theory}$ (ppm)	$\delta(^{27}Al)_{expt}$ (ppm)	molecule	$\delta(^{27}Al)_{theory}$ (ppm)	$\delta(^{27}Al)_{expt}$ (ppm)
$Al^{3+}(H_2O)_6$	0[a]	0[a]	$[(Ox^{2-})Al(OH)_2^{+}(H_2O)_2]$	27	
$[Al^{3+}(H_2O)_6]\cdot 13(H_2O)$			$[(Ox^{2-})Al(OH)_2^{+}(H_2O)]\cdot 2(H_2O)$	53	
$Al(OH)^{2+}(H_2O)_5$	1	3.5[b]	$[(Ox^{2-})Al_2(OH)_4^{2+}(H_2O)_4]$	20	
trans-$Al(OH)_2^{+}(H_2O)_4$	15	3.7[b]	$[(HMalon^{-})Al^{3+}(H_2O)_5]$	6	
"octahedral species"		11.6−11.9[c]	$[(HMalon^{-})_2Al^{3+}(H_2O)_4]$	8	
$[Al(OH)_3(H_2O)]\cdot 2(H_2O)$	70		$[(HMalon^{-})Al(OH)^{2+}(H_2O)_4]$	15	
$[Al(OH)_3(H_2O)_2]\cdot(H_2O)$	48		$[(Malon^{2-})Al^{3+}(H_2O)_4]$	8	
$Al(OH)_3(H_2O)_3$	27		$[(Malon^{2-})_2Al^{3+}(H_2O)_2]$	16	2.5[j]
$[Al(OH)_3(H_2O)_2]\cdot 8(H_2O)$	46		$[(Malon^{2-})_3Al^{3+}]$	9	2.5[j]
$[^{[4]}AlO_4{}^{[6]}Al_{12}(OH)_{24}(H_2O)_{12}]^{7+}$		62.9[d]	$[(H_2Mal^{-})Al^{3+}(H_2O)_5]$	6	
$[Al(OH)_4]^{-}\cdot 2(H_2O)$	78	79.9	$[(H_2Mal^{-})_2Al^{3+}(H_2O)_4]$	7	
$[Al(OH)_4]^{-}\cdot 9(H_2O)$	78		$[(H_2Mal^{-})Al^{3+}(H_2O)_4]$	10	
$[Al_2(OH)_2^{4+}(H_2O)_8]$	3	4.2[c]	$[(H_2Mal^{-})_2Al^{3+}(H_2O)_2]$	20	
$[Al_2(OH)_3^{3+}(H_2O)_7]$	7		$[(HMal^{2-})Al^{3+}(H_2O)_3]\cdot(H_2O)$	33	8[i]
$[Al_2(OH)_4^{2+}(H_2O)_6]$	14		$[(Mal^{3-})Al^{3+}(H_2O)_2]\cdot(H_2O)$	50	
$[Al_2(OH)_5^{+}(H_2O)_5]$	21		$(Mal^{3-})_2{}^{[4]}Al^{3+}]$	83	20[i]
$[Al_2(OH)_6(H_2O)_2]$	26		unknown Al citrate		8[h]
$[(Ac^{-})Al^{3+}(H_2O)_5]$	6	2[e]	unknown Al(OH) citrate		10[h]
$[(Ac^{-})_2Al^{3+}(H_2O)_4]$	10		$[(H_3Cit^{-})Al^{3+}(H_2O)_5]$	6	
$[(Ac^{-})Al^{3+}(H_2O)_4]$[f]	14		$[(H_3Cit^{-})Al(OH)^{2+}(H_2O)_4]$	15	
$[(Ac^{-})_2Al^{3+}(H_2O)_2]$[f]	23		$[(H_2Cit^{2-})Al^{3+}(H_2O)_4]$	13	
$[(Ac^{-})Al(OH)_2^{+}(H_2O)_2]$[f]	32		$[(H_2Cit^{2-})Al(OH)^{2+}(H_2O)_3]$	18	
$[(Ac^{-})Al_2(OH)_2^{4+}(H_2O)_6]$[f]	7		$[(HCit^{3-})^{[5]}Al^{3+}(H_2O)_2]\cdot(H_2O)$	24	
$[(Ac^{-})Al_2(OH)_4^{2+}(H_2O)_4]$[f]	10		$[(Cit^{4-})Al^{3+}(H_2O)_3]$	29	12[h]
$[(HLact^{-})Al^{3+}(H_2O)_5]$	5	6[d]	$[(HCit^{3-})Al^{3+}(H_2O)_3]$[k]	16	
$[(HLact^{-})_2Al^{3+}(H_2O)_4]$	11		$[(Cit^{4-})Al^{3+}(H_2O)_2]\cdot(H_2O)$	32	
$[(HLact^{-})_3Al^{3+}(H_2O)_3]$	7		$[(Cit^{4-})_3Al_3(OH)^{8+}(H_2O)]$	12, 18(2)	
$[(HLact^{-})Al^{3+}(H_2O)_4]$[g]	11	9[h]	$[(Cit^{4-})^{[5]}Al^{3+}(OH)_3]$	58	
$[(HLact^{-})Al^{3+}(H_2O)_4]$[f]	10		$[(HCat^{-})Al^{3+}(H_2O)_5]$	8	
$[(HLact^{-})_2Al^{3+}(H_2O)_2]$[g]	21	15[h]	$[(H_2Cat)Al^{3+}(H_2O)_4]$	2	
$[(HLact^{-})_3Al^{3+}]$[g]	27		$[(H_2Cat)Al(OH)_2^{+}(H_2O)_2]$	18	
$[(Lact^{2-})Al^{3+}(H_2O)_4]$[g]	25	9[d]	$[(Cat^{2-})Al^{3+}(H_2O)_4]$	24	11[l]
$[(Lact^{2-})_2Al^{3+}(H_2O)_2]$[g]	35	15[d]	$[(Cat^{2-})_2Al^{3+}(H_2O)_2]$	32	26[l]
$[(Lact^{2-})_3Al^{3+}]$[g]	31	24[d]	$[(Cat^{2-})_3Al^{3+}]$	28	31.3[l]
$[(HOx^{-})Al^{3+}(H_2O)_5]$	6		$[(Cat^{2-})_2Al(OH)^{2+}]\cdot(H_2O)$	58	32−41[l]
$[(HOx^{-})_2Al^{3+}(H_2O)_4]$	8		$[(Cat^{2-})Al(OH)_2^{+}]$	75	53[l]
$[(HOx^{-})_3Al^{3+}(H_2O)_3]$	16		$[(Cat^{2-})_2Al^{3+}]$	84	58.5[l]
$[(H_2Ox)Al^{3+}(H_2O)_4]$	3		$[(HSal^{-})Al^{3+}(H_2O)_5]$	6	
$[(H_2Ox)_2Al^{3+}(H_2O)_2]$	4		$[(HSal^{-})Al^{3+}(H_2O)_4]$[g]	7	
$[(Ox^{2-})Al^{3+}(H_2O)_4]$	20	6[e]	$[(HSal^{-})Al^{3+}(H_2O)_4]$[f]	16	
$[(Ox^{2-})_2Al^{3+}(H_2O)_2]$	22	12[e]	$[(Sal^{2-})Al^{3+}(H_2O)_4]$[g]	16	3[d]
$[(Ox^{2-})_3Al^{3+}]$	17	16[i]	$[(HSal^{-})Al_2(OH)_2^{4+}(H_2O)_6]$[f]	8	
$[(Ox^{2-})Al(OH)^{2+}(H_2O)_3]$	23		$[(HSal^{-})Al_2(OH)_4^{2+}(H_2O)_4]$[f]	17	

[a] Defined. [b] Reference 23. [c] Reference 54. [d] Reference 22b. [e] Reference 22a. [f] Bonded through two oxygens on the same carboxylate group. [g] Bonded through one carboxylate and one hydroxyl oxygen. [h] Reference 19. [i] Reference 60. [j] Reference 24. [k] Bonded through one oxygen on three carboxylate groups. [l] Reference 21.

HF/6-31G*//3-21G** method, a larger variation was computed with basis sets from HF/3-21G** to HF/6-311+G(3df,2p).[27] On the basis of this earlier work and excluding any $\delta_{iso}(^{27}Al)$ values calculated with the smaller HF/3-21G** basis set, we estimate a maximum error of ±8 ppm (which probably exaggerates the actual uncertainty) for our predictions of $\delta_{iso}(^{27}Al)$ compared to experiment. For most of the measured NMR peaks, this uncertainty will be acceptably small to distinguish among possible complexes.

Al^{3+} Hydrolysis. The ^{27}Al NMR spectra of Al^{3+}-bearing solutions are characterized by the following features: an intense peak at 0 ppm corresponding to the $Al^{3+}(H_2O)_6$ complex, a broadening of the 0 ppm peak and the presence of a weak peak near 3.5−3.7 ppm for solutions with pH > 2, and a sharp peak at 62.9 ppm at pH > 5 assigned to the Al_{13} complex. Another peak around 11.6−11.9 ppm is also observed.[54] The contribution at 3.5−3.7 ppm has been assigned to $Al(OH)^{2+}$, $Al(OH)^{+}{}_2$,[23] and $[Al_2(OH)_2{}^{4+}(H_2O)_8]$[54] species. The calculated $\delta_{iso}(^{27}Al)$ values (Table 3) suggest that $Al(OH)_2^{+}$ has a higher chemical shift than the observed peak at 4 ppm. In addition, the structure of this complex is highly distorted from octahedral symmetry. If present in solution, $Al(OH)_2^{+}$ might not be detectable with NMR spectroscopy. If it is detectable, this species may contribute to the peak observed near 11.6 ppm that has been assigned to "octahedral species".[54] Alternatively, the dimer species $[Al_2(OH)_4{}^{2+}(H_2O)_6]$ could also be responsible for the observed peak near 11.6 ppm. According to our calculations, both the $Al(OH)^{2+}$ and the $[Al_2(OH)_2{}^{4+}(H_2O)_8]$ species could contribute to the observed 3.5−3.7 ppm peak. However, recent calculations with HF/6-31G* geometries and NMR shieldings predict a $\delta_{iso}(^{27}Al)$ of almost 9 ppm for the $Al(OH)^{2+}$ species.[55] If this larger shift is correct, then the observed weak peak near 3.5−3.7 ppm would be due to the $[Al_2(OH)_2{}^{4+}(H_2O)_8]$[54] species. The more deprotonated species listed in Table 3 all have chemical shifts greater than 20 ppm. Except for $[Al(OH)_4]^{-}\cdot 2(H_2O)$, all these species with large shifts are probably too distorted from regular coordination geometries to be observed in NMR spectra.

The effect of adding a second solvation shell around Al^{3+} on calculated ^{27}Al chemical shifts was tested using the complexes $[Al^{3+}(H_2O)_6]\cdot 13(H_2O)$, $[Al(OH)_3(H_2O)_2]\cdot 8(H_2O)$,

and $[Al(OH)_4]^-\cdot 9(H_2O)$. The calculated chemical shielding for the first complex changes by 7 ppm relative to $[Al^{3+}(H_2O)_6]$. Thus, explicit solvation can have a significant effect on the absolute chemical shielding calculated. Chemical shifts calculated for $[Al(OH)_3(H_2O)_2]\cdot 8(H_2O)$ and $[Al(OH)_4]^-\cdot 9(H_2O)$ using $[Al^{3+}(H_2O)_6]$ as the reference are 46 and 78 ppm. The latter value is the same as that calculated for $[Al(OH)_4]^-\cdot 2(H_2O)$, so a second solvation sphere does not affect the chemical shift in this case. The value calculated for $[Al(OH)_3(H_2O)_2]\cdot 8(H_2O)$ is significantly less positive than that predicted for the $[Al(OH)_3(H_2O)]\cdot 2(H_2O)$ complex with only primary solvation. The change is due to the difference in coordination state for these two Al^{3+} ions discussed above. This is not a direct effect of the second solvation sphere however. If eight H-bonded H_2O molecules are removed from the $[Al(OH)_3(H_2O)_2]\cdot 8(H_2O)$ cluster to form $[Al(OH)_3(H_2O)_2]$ and no energy reminimization is calculated, then the calculated $\delta_{iso}{}^{27}Al$ changes by 4 ppm compared to the cluster including the second solvation sphere. This small change in the calculated $\delta_{iso}{}^{27}Al$ due to a second solvation sphere is not enough to significantly affect our conclusions. Hence, we suggest that approximating the chemical environment of Al^{3+} and $Al^{3+}-$organic complexes in solution with only a primary solvation sphere will not fundamentally change our interpretations of the ^{27}Al NMR spectra as discussed below.

$Al^{3+}-$Carboxylate Complexation. Acetate and Lactate. The 2 ppm shift observed for $Al^{3+}-$acetate complexes[22a] is consistent with the values calculated for a 1:1 monodentate complex or possibly the bidentate bridging complex $[(Ac^-)Al_2(OH)_2{}^{4+}(H_2O)_6]$ (Table 3) suggested by Öhman.[56] These results support our contention that our model calculations are able to reproduce $\delta_{iso}(^{27}Al)$ values within at least ± 8 ppm because the most probable model species give $\delta_{iso}(^{27}Al)$ values within $4-5$ ppm of the measured value. Unfortunately, the NMR results alone are not enough to distinguish these two assignments. Vibrational spectra of $Al-$acetate complexes in solution would be useful in this regard to test if either of these complexes produces vibrational frequencies consistent with measured values as well as the ^{27}Al chemical shifts.

$Al^{3+}-$lactate complexation provides the opportunity to test our methodology and previous assignments, because a number of peaks have been detected at different Al/lactate ratios. A 6 ppm peak has been assigned to a 1:1 monodentate $Al^{3+}-$lactate complex (Figure 2a[22b]), and our calculations confirm this assignment within 1 ppm (Table 3). A second peak at 9 ppm has been interpreted either as a $[(HLact^-)Al^{3+}(H_2O)_4]$ (Figure 2b[19]) or $[(Lact^{2-})Al^{3+}(H_2O)_4]$ bidentate species (Figure 2c[22b]). Calculated results in Table 3 are consistent with the former interpretation with the latter complex giving a model value of $+25$ ppm. Other species with calculated chemical shifts within error of the experimental value of 9 ppm are $[(HLact^-)Al^{3+}(H_2O)_4]$ (Figure 2d), $[(HLact^-)_2Al^{3+}(H_2O)_4]$ (Figure 2e), and $[(HLact^-)_3Al^{3+}(H_2O)_3]$. The first of these is unlikely to form due to strain energy associated with forming the $Al^{3+}-O-C-O$ ring.[57] The latter two monodentate species are not prohibited energetically and may form and contribute to observed NMR intensity near 9 ppm depending on the lactate/Al^{3+} ratio of the solution. Within our error, the chemical shifts calculated at 11 ppm could also be responsible for the observed 15 ppm peak. Karlik et al.[19] assigned this band to a bidentate $[(HLact^-)_2Al^{3+}(H_2O)_2]$ species, whereas Thomas et al.[22b] suggested a bidentate $[(Lact^{2-})_2Al^{3+}(H_2O)_2]$. Our results are more consistent with the former interpretation because the difference between experiment and theory is 6 ppm for $[(HLact^-)_2Al^{3+}(H_2O)_2]$, but the difference is 20 ppm for the latter complex (Table 3). Last, a peak at 24 ppm was observed by Thomas et al.[22b] and assigned to a $[(Lact^{2-})_3Al^{3+}]$ complex. The calculated $\delta_{iso}(^{27}Al)$ value for this complex is in marginal agreement with the experimental assignment (Table 3), so we cannot rule out this possibility. Other candidates are the bidentate $[(Lact^{2-})Al^{3+}(H_2O)_4]$ (25 ppm), protonated bidentate $[(HLact^-)_2Al^{3+}(H_2O)_2]$ (21 ppm), and protonated bidentate $[(HLact^-)_3Al^{3+}]$ (27 ppm) complexes. This last complex has been observed in crystals precipitated from $Al^{3+}-$lactate solutions.[58] Without other constraints, such as vibrational spectra, we cannot distinguish which of these species is most probable.

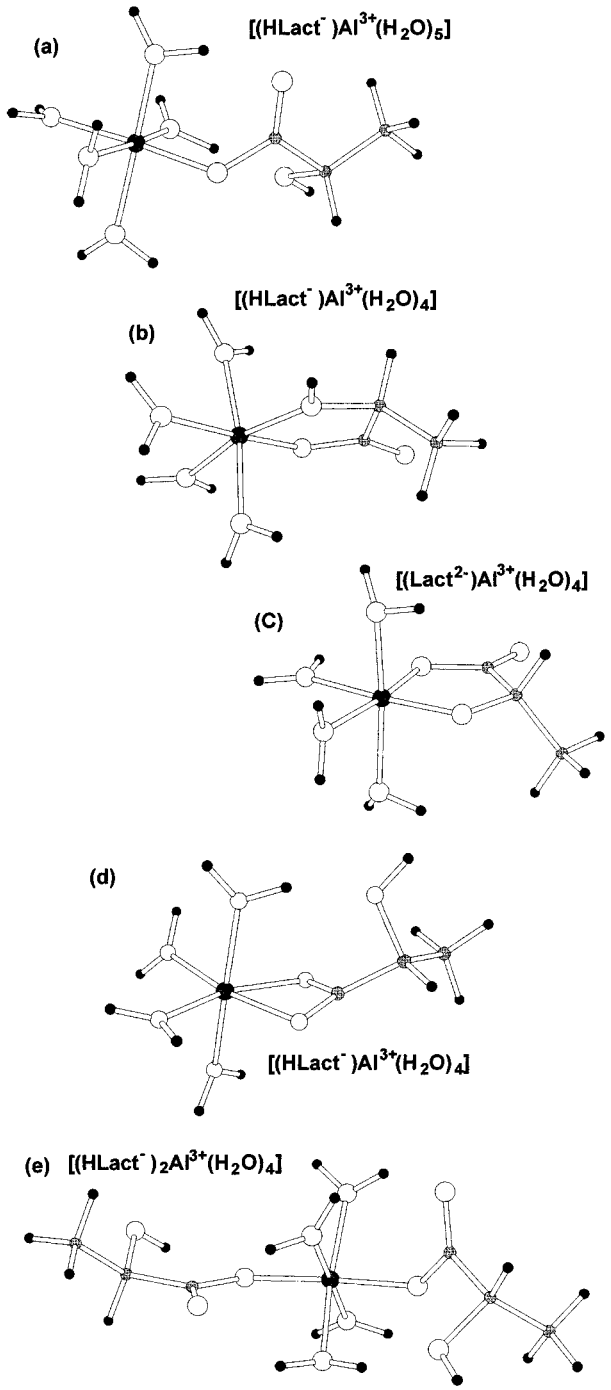

Figure 2. (a) $[(HLact^-)Al^{3+}(H_2O)_5]$; (b) $[(HLact^-)Al^{3+}(H_2O)_4]$; (c) $[(Lact^{2-})Al^{3+}(H_2O)_4]$; (d) $[(HLact^-)Al^{3+}(H_2O)_4]$ (bidentate 2 configuration); (e) $[(HLact^-)_2Al^{3+}(H_2O)_4]$. Molecules drawn with the program Atoms.[70] H are black, O are white, C are light gray, and Al are dark gray.

To summarize, the species proposed by Thomas et al.[22b] to explain the peaks at 6, 9, 15, and 24 ppm have calculated chemical shifts of 5 ppm ($[(HLact^-)Al^{3+}(H_2O)_5]$), 25 ppm ($[(Lact^{2-})Al^{3+}(H_2O)_4]$), 35 ppm ($[(Lact^{2-})_2Al^{3+}(H_2O)_2]$), and 31 ppm ($[(Lact^{2-})_3Al^{3+}]$). Similarly, the species proposed by Karlik et al.[19] for the peaks at 9 and 15 ppm have calculated shifts of 11 ppm ($[(HLact^-)Al^{3+}(H_2O)_4]$) and 21 ppm ($[(HLact^-)_2Al^{3+}(H_2O)_2]$). On the basis of the current calculations, we assign the observed peaks at 6, 9, 15, and 24 ppm to $[(HLact^-)Al^{3+}(H_2O)_5]$, $[(HLact^-)_2Al^{3+}(H_2O)_4]$, $[(HLact^-)_2Al^{3+}(H_2O)_2]$, and $[(HLact^-)_3Al^{3+}]$, respectively. However, the last assignment is the most tenuous of the three because other model complexes result in similar calculated $\delta_{iso}(^{27}Al)$ values.

Oxalate, Malonate, Malate, and Citrate. An accuracy test of the HF/6-31G* calculations was performed in this study using HF/6-31G(2d) and HF/6-311+G** basis sets on the same molecular structure for $[(Ox^{2-})Al^{3+}(H_2O)_4]$ as presented in Table 3. The larger basis sets give δ^{27}Al values of 22 and 25 ppm, respectively, compared to the 20 ppm value calculated with HF/6-31G*. Furthermore, density functional theory calculations using the Becke[43] exchange functional and the Perdew−Wang[59] gradient-corrected correlation functional and the 6-311+G** basis set on $[Al^{3+}(H_2O)_6]$ and $[(Ox^{2-})Al^{3+}(H_2O)_4]$ predicted a δ^{27}Al of 24 ppm. We conclude that the Al^{3+}−carboxylate values calculated in this study would change by less than ±8 ppm if a larger basis set were used to calculate the chemical shieldings. Furthermore, these calculations with larger basis sets give the model-predicted values farther from the experimental value rather than closer to it. Since it was demonstrated in Sykes et al.[27] that larger basis sets do not necessarily result in more accurate chemical shift predictions, we have decided to use the HF/6-31G* basis set for ^{27}Al chemical shift calculation and accept a ±8 ppm uncertainty in our results.

NMR spectra of Al^{3+}−oxalate solutions have peaks at 6, 12,[22a] and 16 ppm[60] depending on the Al/oxalate ratio. Peak assignments are based on bidentate Al^{3+}−oxalate species with the above bands assigned to $[(Ox^{2-})Al^{3+}(H_2O)_4]$, $[(Ox^{2-})_2Al^{3+}(H_2O)_2]$, and $[(Ox^{2-})_3Al^{3+}]$, respectively. Calculated chemical shifts for the first two model complexes (20 and 22 ppm, respectively) are outside the range of uncertainty compared with the experimental values (Table 3). Monodentate $[(HOx^-)Al^{3+}(H_2O)_5]$ and $[(HOx^-)_2Al^{3+}(H_2O)_4]$ species provide theoretical chemical shifts much closer to the experimental values (6 and 8 ppm, respectively). Protonated bidentate $[(H_2Ox)Al^{3+}(H_2O)_4]$ and $[(H_2Ox)_2Al^{3+}(H_2O)_2]$ species also result in theoretical chemical shifts more consistent with observed values (Table 3). The third peak at 16 ppm could be due to either a monodentate $[(HOx^-)_3Al^{3+}(H_2O)_3]$ or bidentate $[(Ox^{2-})_3Al^{3+}]$ species according to our results. The latter species is the stable form upon crystallization[61] and thus seems the most probable.

To distinguish the correct assignment for these Al−oxalate peaks, we have also examined calculated ^{17}O chemical shifts in relation to the observed values. Phillips et al.[62] measured ^{17}O NMR spectra of Al−oxalate solutions. These authors found a sharp peak and a broad peak both centered near 22 ppm that were assigned to O atoms in water molecules of the complexes $[Al^{3+}\cdot 6(H_2O)]$ and $[(Ox^{2-})Al^{3+}(H_2O)_4]$, respectively. Calculated ^{17}O chemical shieldings using the HF/6-31+G* (a diffuse function, "+", was added to this calculation to better describe the electron density around the oxygen atoms) basis set average 315 ppm for a $(H_2O)_9$ cluster and 317 ppm for $[Al^{3+}\cdot 6(H_2O)]$. This model chemical shift of −2 ppm is too small and in the wrong direction compared to the measured +22 ppm shift. On the other hand, a larger cluster of $[Al^{3+}\cdot 19(H_2O)]$ predicts average chemical shieldings of 325 and 303 ppm for the free and bound water molecules, respectively. Thus, the calculated chemical shift for oxygen atoms in water molecules bound to an Al^{3+} ion in this case is +22 ppm, perhaps fortuitously close to the measured value.[62] As another test of the accuracy of these calculations, the ^{17}O chemical shift for carboxylate oxygens of oxalate in solution are found at 253 ppm.[60] In the clusters $HOx^-\cdot 8(H_2O)$ and $Ox^{2-}\cdot 8(H_2O)$, the calculated chemical shifts are 240−260 and 235−250 ppm, respectively. Both of these ranges are reasonably close to the measured value.

The calculated ^{17}O chemical shift for bound water in $[(Ox^{2-})Al^{3+}(H_2O)_4]$ (the assigned complex to the broad band near 22 ppm) is 10−15 ppm, but similar values are also calculated for bound waters in the monodentate $[(HOx^-)Al^{3+}(H_2O)_5]$ and protonated bidentate $[(HOx^-)Al^{3+}(H_2O)_4]$ complexes. Thus, we cannot distinguish among three 1:1 Al−oxalate complexes based on the peaks near 22 ppm. Two other peaks were observed at 232 and 245 ppm and assigned to carboxyl oxygens in the bidentate $[(Ox^{2-})Al^{3+}(H_2O)_4]$ and $[(Ox^{2-})_2Al^{3+}(H_2O)_2]$ complexes, respectively. However, calculated chemical shifts for the oxygen atoms in the C−O−Al linkages of these complexes are 148 and 175 ppm, respectively. The only calculated ^{17}O chemical shifts that lie near the observed peaks at 232 and 245 ppm are from the monodentate Al−trioxalate species $[(HOx^-)_3Al^{3+}(H_2O)_3]$, and these range from 219 to 246 ppm. This species also had a calculated ^{27}Al chemical shift consistent with a measured peak at 16 ppm. The bidentate trioxalate species, $[(Ox^{2-})_3Al^{3+}]$, has a calculated ^{17}O chemical shift of 204 ppm for the C−O−Al oxygen atom, which is farther from the observed value. Monodentate $[(HOx^-)_3Al^{3+}(H_2O)_3]$ is thus consistent with both the ^{17}O and ^{27}Al NMR spectra. Protonated bidentate species are consistent with the ^{27}Al but not the ^{17}O NMR spectra. Bidentate complexes have calculated δ^{27}Al and δ^{17}O values that are consistent with neither spectrum.

Another check on our assignment of the NMR peaks can be made by comparing model and observed vibrational spectra of similar solutions. Raman spectra of Al−oxalate solutions have been measured by Jaber et al.[64] in solutions that ranged from Al/oxalate ratios of 1/3 to 1 and pH conditions of ≈ 0 to 6.3. Observed peaks assigned to oxalate vibrations occurred at 1278, 1408, 1423−1429, 1486 (pH 6.3 only), 1686−1698, 1723−1733, and 1746−1750 cm^{-1}. For comparison, the bidentate complexes $[(Ox^{2-})Al^{3+}(H_2O)_4]$, $[(Ox^{2-})_2Al^{3+}(H_2O)_2]$, and $[(Ox^{2-})_3Al^3]$ have predicted frequencies of 1272−1299, 1308−1332, 1386−1405, 1662−1679, 1716−1734, 1745−1760, and 1783−1798 cm^{-1}. Hence, there is reasonable agreement between the observed and modeled frequencies for the bidentate complexes except for the observed 1423−1429 and 1486 cm^{-1} bands. Also, there are no bands observed near 1308−1332 or 1783−1798 that were calculated for the $[(Ox^{2-})_2Al^{3+}(H_2O)_2]$ and $[(Ox^{2-})Al^{3+}(H_2O)_4]$ complexes, respectively. In the model monodentate complexes, predicted frequencies are 1261, 1364−1388, 1425−1466, 1641, 1661−1678, 1694, 1766−1772, and 1806 cm^{-1}. The agreement between theory and experiment here is similar to that found for the bidentate complexes. However, calculated bands at 1364−1388, 1641, and 1806 cm^{-1} exist that are not observed. Unobserved bands are simple to explain if the vibrations are merely weak Raman scatterers. More difficult to explain are the cases where bands are observed but none are predicted as is the case for the 1408 and 1723−1733 cm^{-1} bands missing from the monodentate complex calculated spectra or the 1423−1429 and 1486 cm^{-1} bands missing from the bidentate complex calculated spectra. Since these missing bands can be

explained by a combination of the monodentate and bidentate complex spectra, it may be possible that a mixture of complexes exists in these solutions. Alternatively, some of the missing bands may be explained by protonated bidentate species such as $[(H_2Ox)Al^{3+}(H_2O)_4]$ and $[(H_2Ox)_2Al^{3+}(H_2O)_2]$ that have model frequencies in the range of 1364−1372, 1391−1408, 1854−1856, and 1882−1887.

For Al^{3+}−malonate aqueous complexes, we know of only one measured peak at 2.5 ppm. This has been assigned to both Al^{3+}−dimalonate and Al^{3+}−trimalonate with bidentate configurations.[24] Thermodynamic calculations predict that the dominant species in solution changes from Al^{3+}−dimalonate to Al^{3+}−trimalonate over the pD range (pD 3.77 to 7.52) of the NMR spectra.[24] Hence, the authors concluded that both species have the same δ^{27}Al. Our results cannot rule out the possibility that the Al^{3+}−trimalonate species, $[(Malon^{2-})_3Al^{3+}]$, gives rise to the 2.5 ppm peak, but the monodentate Al^{3+}−malonate species, $[(HMalon^{1-})Al^{3+}(H_2O)_5]$, does give somewhat better agreement with experiment (Table 3). Furthermore, our results suggest that it is unlikely that both the Al^{3+}−dimalonate and Al^{3+}−trimalonate complexes have the same δ^{27}Al value since the model results are separated by 7 ppm (Table 3).

As a check on our ^{27}Al calculations, we have also examined the calculated δ^{13}C values in light of the available experimental spectra.[24] The ^{13}C NMR spectra of the same solutions show a +0.4 ppm difference between the δ^{13}C values for carboxylate groups in all solutions over the range of aluminum/malonic acid ratios in the study.[24] Our calculations show a +5 ppm difference between the C atoms in carboxylate groups of the Al^{3+}−dimalonate and Al^{3+}−trimalonate complexes. The difference in the carboxylate δ^{13}C values between the monodentate $[(HMalon^{1-})Al^{3+}(H_2O)_5]$ and the bidentate $[(Malon^{2-})Al^{3+}(H_2O)_4]$ species of 0.8 ppm is more consistent with the ^{13}C NMR spectra. These two species also have calculated δ^{27}Al values somewhat closer to experiment and to each other (2 ppm); hence, both the ^{27}Al and ^{13}C NMR spectra can be more accurately reproduced with these species rather than bidentate Al^{3+}−dimalonate and Al^{3+}−trimalonate. These discrepancies could be caused by errors in our computational methodology, errors in modeling the thermodynamics of these solutions, or a lack of equilibrium between Al−malonate species in solution. This last explanation seems the most likely. An Al^{3+}−dimalonate complex has a square planar configuration for the ligands with two water molecules in axial positions.[24] To form Al^{3+}−trimalonate, one of the Al−malonate bonds must be broken, because a single malonate molecule cannot bond at the two axial sites simultaneously. Lack of equilibrium in solution could be a common cause of misassignments for observed spectroscopic peaks particularly with strongly bonded ligands where activation barriers may need to be overcome to form new species.

Experimental assignments for ^{27}Al NMR spectra of Al^{3+}−malate aqueous complexes are based on bidentate and tridentate species.[63] Model results predict chemical shifts that are significantly larger than the observed values (Table 3). Monodentate $[(H_2Mal^{-})Al^{3+}(H_2O)_5]$ and $[(H_2Mal^{-})_2Al^{3+}(H_2O)_4]$ complexes and a bidentate $[(H_2Mal^{-})Al^{3+}(H_2O)_4]$ complex are more consistent with the first peak observed at 8 ppm (Table 3). A bidentate complex, $[(H_2Mal^{-})_2Al^{3+}(H_2O)_2]$, with an Al^{3+}−(OH)−C linkage similar to that found in Figure 2b for Al^{3+}−lactate complexation, has a predicted chemical shift of 20 ppm that may be assigned to the observed peak at 20 ppm.

^{27}Al NMR spectra of Al^{3+}−citrate solutions have been measured by Karlik et al.[19] These authors noted three peaks at 8, 10, and 12 ppm, but only the 12 ppm peak was given a definite assignment due to the number of Al^{3+}−citrate configurations possible. The 12 ppm peak was assigned to a 1:1 Al^{3+}−citrate complex with the Al^{3+} bound to two carboxyl oxygens and one hydroxyl oxygen, a configuration that has two six-membered rings.

Two attempts were made to find a stable complex with this configuration. During the energy minimization, the complex $[(Cit^{4-})Al^{3+}(H_2O)_3]$ was driven into a quadradentate configuration as the initially free COO^- group displaced a water molecule from coordination around Al^{3+}. The calculated δ^{27}Al for the quadradentate $[(Cit^{4-})Al^{3+}(H_2O)_2]\cdot(H_2O)$ is +29 ppm, so this complex is unlikely to give rise to the 12 ppm peak. Since the COO^- group in the citrate molecule that was initially not bonded to Al^{3+} caused displacement of the H_2O, a second complex with this free COO^- group protonated ($[(Cit^{3-})Al^{3+}(H_2O)_3]$) was also energy minimized. In this case, a H_2O molecule was also displaced and a pentacoordinate Al^{3+} was formed. However, the carboxyl group in this case formed what could be considered a long sixth bond at about 2.2 Å, so this complex could also be considered a highly distorted octahedral coordination. The δ^{27}Al calculated for $[(Cit^{3-})Al^{3+}(H_2O)_2]\cdot(H_2O)$ was 24 ppm (Table 3), which is inconsistent with the measured 12 ppm value.

Feng et al.[65] have proposed that the $[(Cit^{4-})_3Al_3{}^{3+}(OH)(H_2O)]$ complex is a stable species in solution. The structure of this large cluster is clearly described by Powell and Heath.[66] A minimum energy configuration of this complex was found with the HF/3-21G** basis set (Note: A force constant analysis was not completed for this large cluster). NMR calculations with the HF/6-31G* basis set predict a δ^{27}Al value of 12 ppm for one Al^{3+} and 18 ppm for the other two. Thus, the former value is in good agreement with the peak at 12 ppm measured for Al^{3+}−citrate complexes in solution.[19]

A complex that may explain the observed peak at 8 ppm is the monodentate $[(H_3Cit^{-})Al^{3+}(H_2O)_5]$ complex (Table 3). The monodentate $[(H_3Cit^{-})Al(OH)^{2+}(H_2O)_4]$, bidentate $[(H_2Cit^{2-})Al^{3+}(H_2O)_4]$, or tridentate $[(HCit^{3-})Al^{3+}(H_2O)_3]$ species with calculated δ^{27}Al values of 15, 13, and 16 ppm, respectively, could give rise to the observed peaks at 10 or 12 ppm. All of these configurations are different from what has been suggested previously. There are no bonds through the hydroxyl oxygen on the citrate ligand. Complexes that are bonded through the hydroxyl oxygen give much larger calculated chemical shifts. Furthermore, these calculations suggest that Al^{3+}−OH_2 groups should deprotonate before the hydroxyl group and the third carboxyl group because complexes such as $[(H_2Cit^{2-})Al^{3+}(H_2O)_5]$ undergo proton transfers to become $[(H_3Cit^{-})Al(OH)^{2+}(H_2O)_4]$. These results suggest that a re-evaluation of Al^{3+}−citrate complexation mechanisms would be worthwhile.

Catecholate and Salicylate. Numerous ^{27}Al NMR bands due to Al^{3+}−catecholate aqueous complexes are noted by Mhatre et al.[60] In Table 3, each of these peaks and the corresponding experimental assignments are listed and compared to calculated values for each proposed complex. The first peak at 11 ppm was assigned to a $[(Cat^{2-})Al^{3+}(H_2O)_4]$ bidentate complex. Model results predict a chemical shift of 24 ppm for this complex. Closer agreement is found with the $[(HCat^{-})Al^{3+}(H_2O)_5]$ monodentate complex. The calculated chemical shift for the $[(Cat^{2-})Al^{3+}(H_2O)_4]$ is actually closer to the second observed peak at 26 ppm[60] (Table 3). A bidentate Al^{3+}−tricatecholate complex also gives a model chemical shift close to this value (28 ppm), but this assignment is less probable for the 26 ppm

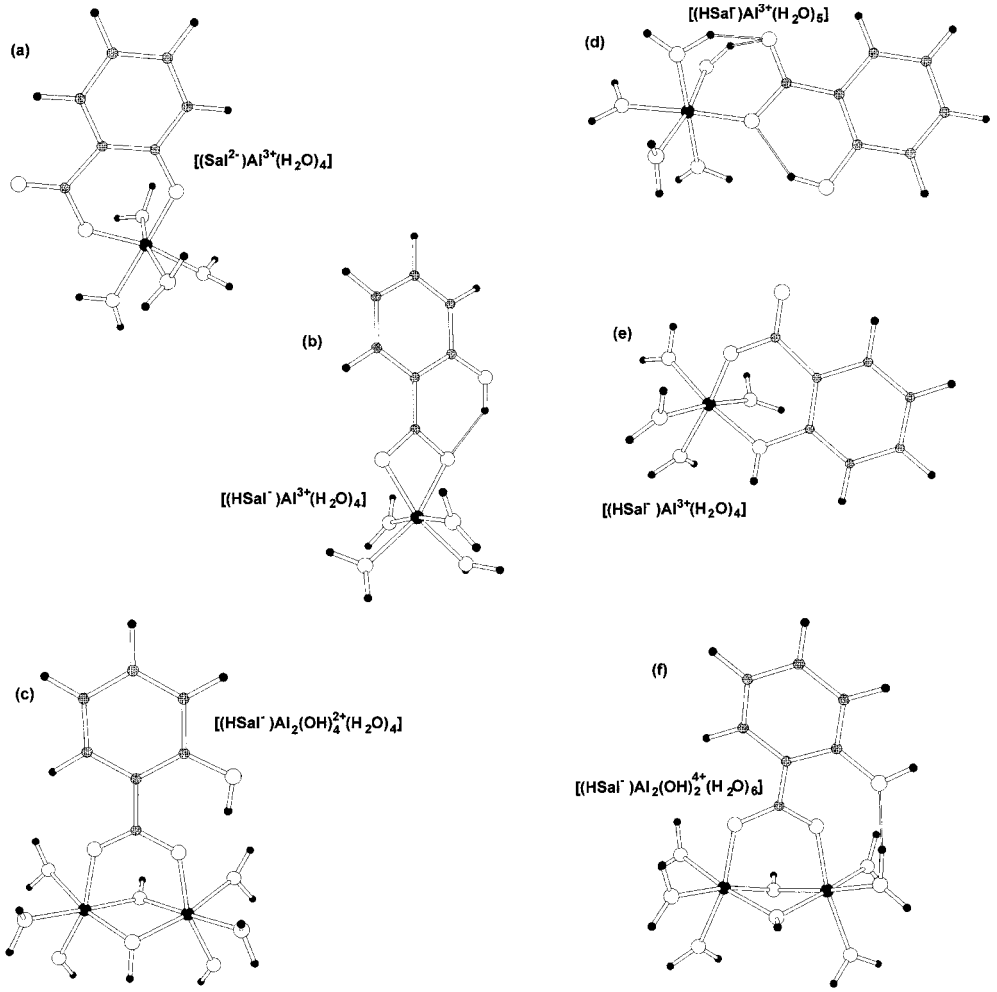

Figure 3. (a) $[(Sal^{2-})Al^{3+}(H_2O)_4]$; (b) $[(HSal^{-})Al^{3+}(H_2O)_4]$ (bidentate 2 configuration); (c) $[(HSal^{-})Al_2(OH)_4^{2+}(H_2O)_4]$ (bidentate bridging configuration); (d) $[(HSal^{-})Al^{3+}(H_2O)_5]$; (e) $[(HSal^{-})Al^{3+}(H_2O)_4]$ (protonated bidentate configuration); (f) $[(HSal^{-})Al_2(OH)_2^{4+}(H_2O)_6]$ (bidentate bridging configuration). Molecules drawn with the program Atoms.[70] H are black, O are white, C are light gray, and Al are dark gray.

peak because it occurs at low catechol/Al^{3+} ratios.[60] A more likely scenario is that the $[(Cat^{2-})_2Al^{3+}(H_2O)_2]$ ($\delta_{calc}(^{27}Al)$ = 32 ppm) and $[(Cat^{2-})_3Al^{3+}]$ give rise to the peaks at 31 to 32 ppm that are found at higher catechol/Al^{3+} ratios.[60] Peaks at 53 and 58.5 ppm have also been detected experimentally[60] and assigned to the tetrahedral aluminum species $[(Cat^{2-})^{[4]}Al(OH)_2^{+}]$ and $[(Cat^{2-})_2^{[4]}Al^{3+}]$, respectively. Both of these tetrahedral species have calculated chemical shifts closer to that of the ^{27}Al NMR standard $[Al(OH)_4]^{-}$ (Table 3). A complex with a calculated chemical shift more consistent with the observed 53 and 58.5 ppm peaks is the pentacoordinate complex $[(Cat^{2-})_2^{[5]}Al(OH)^{2+}]$, with a theoretical $\delta_{calc}(^{27}Al)$ = 58 ppm. To our knowledge, pentacoordinate Al^{3+} has not been suggested previously to explain ^{27}Al NMR spectra of aqueous solutions. However, we have also predicted a pentacoordinate Al^{3+} configuration for the $Al(OH)_3$ aqueous species (see Al Hydrolysis Section) which has a similar calculated d(^{27}Al) (Table 3).

One broad shoulder at 3 ppm has been reported for ^{27}Al NMR spectra of acidic Al^{3+}−salicylate solutions.[22b] These authors assigned the peak to a bidentate 1:1 Al^{3+}−salicylate complex with bonding through one carboxylate oxygen and one phenol oxygen (Figure 3a). Calculated results predict that this and other bidentate complexes (Figure 3a−c) would have $\delta(^{27}Al)$ values equal to 16−17 ppm. In contrast, the monodentate $[(HSal^{-})Al^{3+}(H_2O)_5]$, protonated bidentate $[(HSal^{-})Al^{3+}(H_2O)_4]$, and bridging bidentate $[(Sal^{-})Al_2(OH)_2^{4+}(H_2O)_6]$ complexes (Figure 3d−f) have model chemical shifts of 6−8 ppm, much closer to the observed experimental value. Given the broad nature of the observed band and the ±8 ppm uncertainty in our calculations with regard to reproducing experimental values, any of these three complexes could be responsible for the observed band.

To reduce the number of possible complexes assigned to the NMR peak, we compared the observed infrared frequencies for aqueous Al^{3+}−salicylate solutions[67] to frequencies calculated for the model complexes listed in Table 3 and shown in Figure 3d−f. Figure 4 correlates these experimental frequencies and the model values for each complex. The closest fit to the measured frequencies is provided by the monodentate $[(HSal^{-})Al^{3+}(H_2O)_5]$ complex with a slope of 1.02 ± 0.02, an intercept of −40 ± 36 cm^{-1}, and an R^2 value of 0.996. Considering the approximations made using a small basis set and comparing gas-phase calculations to aqueous-phase experiments, this agreement is excellent. Correlations of frequencies calculated based on the bidentate complexes, $[(HSal^{-})Al^{3+}(H_2O)_4]$ and $[(Sal^{-})Al_2(OH)_2^{4+}(H_2O)_6]$, with experiment result in slopes of 1.12 ± 0.04 and 0.88 ± 0.06, respectively, larger variations from the ideal 1.0 value than the 1.02 value for $[(HSal^{-})Al^{3+}(H_2O)_5]$. In addition, the intercepts of these two correlations derived from bidentate complexes are −173 ± 62 and 152 ± 86 cm^{-1}, respectively, significantly in error from 0. Hence, we suggest that the monodentate $[(HSal^{-})Al^{3+}(H_2O)_5]$ complex is the best assignment for the observed NMR and IR spectra of acidic Al−salicylate solutions.[22b,67]

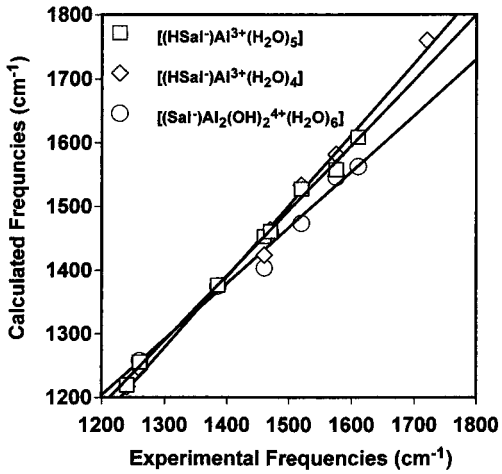

Figure 4. Comparison of calculated vibrational frequencies for three possible Al−salicylate complexes to observed infrared peaks for Al−salicylate solutions.[67]

Discussion

To demonstrate the relevance of our calculations to the ^{27}Al NMR spectra of Al^{3+} in solution, we have shown that model clusters with a single solvation sphere can reproduce the δ^{27}Al between the standards $Al^{3+}_{(aq)}$ and $[Al(OH)_4]^-_{(aq)}$ within reasonable accuracy. Furthermore, calculations on other model clusters (e.g., $[Al(OH)^{2+}(H_2O)_5]$ and $[Al_2(OH)_2{}^{4+}(H_2O)_8]$) likely to exist in Al^{3+}-bearing aqueous solutions also predict δ^{27}Al values corresponding to observed peaks. In systems such as Al^{3+}−acetate, where complexation mechanisms are readily interpreted due to the simple nature of the ligand, agreement is also good between experimental peak assignments and model calculations.

Our modeling results suggest that complexation mechanisms involving bonding a L^{2-} or L^{3-} ligand in a bidentate or tridentate manner to Al^{3+} results in chemical shifts that are generally larger than those observed experimentally. In fact, the environment surrounding the Al^{3+} cation can be highly distorted in this type of complex, which could make the ^{27}Al difficult to detect with NMR spectroscopy.[68] Distortion is so high in some complexes that coordination changes to either 5-fold or 4-fold coordination is predicted. Thus, the chemical shifts would be found in the range 50−80 ppm, well outside the broad bands generally observed from 0 to 30 ppm.

Monodentate complexes or bidentate species with protonated Al^{3+}−(OH)−C linkages (e.g., Figures 2a,b and 3d,e) generally have calculated ^{27}Al chemical shifts that correspond better to observed values in Al^{3+}−carboxylic acid solutions. Calculated energy differences between these two types of complexes are small with the monodentate configurations approximately 10 kJ/mol lower in potential energy. However, formation of the bidentate species should lead to a positive entropy change as a water molecule is released from coordination around Al^{3+}. Shock and Koretsky[69] have suggested that the ΔS for this type of reaction is approximately 70 J/(mol K). At 300 K, this translates into −21 kJ/mol of Gibbs free energy and would make the reaction from monodentate to protonated bidentate species favorable by approximately −10 kJ/mol. Although the proton in the Al^{3+}−(OH)−C linkage is acidic, calculated deprotonation energies for these species can be higher than steps in the Al^{3+} hydrolysis series. For example, $[(HLact^-)Al^{3+}(H_2O)_4] + H_2O\cdot 8(H_2O) \rightarrow [(Lact^{2-})Al^{3+}(H_2O)_4] + H_3O^+\cdot 8(H_2O)$ (Table 2) is predicted to have a ΔE of +22 kJ/mol. Compared to +8 kJ/mol for $[Al^{3+}(H_2O)_6] + H_2O\cdot 8(H_2O) \rightarrow [Al(OH)^{2+}(H_2O)_5] + H_3O^+\cdot 8(H_2O)$, the proton in the Al^{3+}−(OH)−C would be more difficult to remove and would not deprotonate at pH's where $[Al^{3+}(H_2O)_6]$ was a stable species.

If equilibrium exists between the monodentate and protonated bidentate species and deprotonation of this latter type of complex occurs as pH increases, then bidentate species with L^{2-} ligands are likely to be stable at neutral pH's. Unfortunately, these complexes may not be detected with NMR because most NMR spectra of Al^{3+}−carboxylic acid solutions are collected under acidic conditions (~pH 3 or less) to prevent polymerization and precipitation of Al hydroxides.[22a] Even when ^{27}Al NMR spectra are collected at low total Al^{3+} concentrations to avoid precipitation[23] under neutral conditions, NMR peaks may not be detected due to the highly distorted nature of the complex. As a general rule, we would predict that complexes with two or more strong Al^{3+}−O bonds lengthen the remaining Al^{3+}−OH_2 bonds and distort the complex from octahedral symmetry. If species such as $[(Ox^{2-})_3Al^{3+}]$ form however, octahedral symmetry is regained because all six Al^{3+}−O bonds are equivalent. ^{27}Al NMR spectra may detect these species, and our calculations predict chemical shifts that are compatible with observed experimental values. When a Al^{3+}−tricarboxylate species is stable, such as $[(Ox^{2-})_3Al^{3+}]$, then these species may form even at low carboxylate/Al^{3+} ratios. Once the 1:1 Al^{3+}−carboxylate complex is formed in solution, the remaining Al^{3+}−(OH_2) bonds lengthen, making their replacement by other ligands more favorable.[62] Thus, the 1:1 and 1:2 Al^{3+}−carboxylate species may not be detected in solutions where the 1:3 complex can form. However, this transition to bidentate species is complicated by possible oligomerization at higher pH. Consequently, additional spectroscopy, such as infrared and Raman, and model calculations may be necessary to unravel the Al−carboxylate speciation in aqueous solutions.

Conclusion

We have tested the methodology used in our modeling study with a variety of comparisons to experimental data. In each case, reasonable agreement indicates that the calculations on small molecular clusters model the essential aspects of Al^{3+} and Al^{3+}−carboxylic acid chemistry in aqueous solutions. Some discrepancies exist between the experimental interpretation of ^{27}Al NMR spectra and model results based on bidentate and tridentate complexes. In most cases, these differences can be explained by protonation of the carboxylate anion either forming a monodentate or protonated bidentate complex to lower the calculated chemical shift. Large chemical shifts due to the deprotonated bidentate complexes should be difficult to detect with ^{27}Al NMR spectroscopy due to the large distortions from octahedral symmetry that occur with formation of covalent bonds between Al^{3+} and the carboxylate anions.

Acknowledgment. The authors appreciate the time and effort put into the review process by Jack Tossell and an anonymous reviewer. S.E.A. and J.D.K. acknowledge the financial support of ONT and ONR. Computer resources were supplied by the DoD HPC initiative through the Space and Naval Warfare Systems Center, San Diego, CA and the Aeronautical Systems Center, Dayton, OH.

References and Notes

(1) Vik, E. A.; Eikebrokk, B. In *Aquatic Humic Substances*; Suffet, I. H., MacCarthy, P., Ed.; American Chemical Society: Washington, DC, 1989; p 385.

(2) Dempsey, B. A. In *Aquatic Humic Substances*; Suffet, I. H., MacCarthy, P., Eds.; American Chemical Society: Washington, DC, 1989; p 409.

(3) Bottero, J. Y.; Bersillon, J. L. In *Aquatic Humic Substances*; Suffet, I. H., MacCarthy, P., Eds.; American Chemical Society: Washington, DC, 1989; p 425.
(4) Hue, N. V.; Craddock, G. R.; Adams, F. *Soil Sci. Soc. Am. J.* **1986**, *50*, 28.
(5) Sunda, W. G.; Tester, P. A.; Huntsman, S. A. *Estuarine, Coastal, and Shelf Sci.* **1990**, *30*, 207.
(6) Parker, D. R.; Bertsch, P. M. *Environ. Sci. Technol*. **1992**, *26*, 908.
(7) Underdown, A. W.; Langford, C. H.; Gamble, D. S. *Environ. Sci. Technol*. **1985**, *19*, 132.
(8) Jones, K. D.; Tiller, C. L. *Abstr. Papers ACS* **1996**, *211*, ENVR-31.
(9) Herbes, S. E.; Schwall, L. R. *Appl. Environ. Microbiol.* **1978**, *35*, 306.
(10) Paul, E. A.; Clark, F. E. *Soil Microbiology and Biochemistry*; Academic Press: San Diego, CA, 1989.
(11) Furrer, G.; Stumm, W. *Geochim. Cosmochim. Acta* **1986**, *50*, 1847.
(12) Welch, S. A.; Ullman, W. J. *Geochim. Cosmochim. Acta* **1993**, *57*, 2725.
(13) Fein, J. B.; Hestrin, J. E. *Geochim. Cosmochim. Acta* **1994**, *58*, 4817.
(14) Eberl, D. D. *Clays Clay Miner.* **1993**, *41*, 26.
(15) Fein, J. B. *Chem. Geol.* **1994**, *115*, 263.
(16) Schindler, P. W.; Stumm, W. *Aquatic Surface Chemistry−Chemical Processes at the Particle−Water Interface*; Wiley: New York, 1987; p 83.
(17) Casey, W. H.; Ludwig, C. In *Chemical Weathering Rates in Silicate Minerals*; White, A. F., Brantley, S. L., Eds.; Mineralogical Society of America: Washington, DC, 1995; p 87.
(18) (a) Murphy, E. M.; Zachara, J. M.; Smith, S. C. *Environ. Sci. Technol.* **1990**, *24*, 1507. (b) Murphy, E. M.; Zachara, J. M.; Smith, S. C.; Phillips, J. L. *Sci. Total Environ.* **1992**, *117/118*, 413.
(19) Karlik, S. J.; Tarien, E.; Elgavish, G. A.; Eichhorn, G. L. *Inorg. Chem*. **1983**, *22*, 525.
(20) Akitt, J. W. *Prog. NMR Spectrosc.* **1989**, *21*, 1.
(21) Mhatre, S. N.; Karweer, S. B.; Pradhan, P.; Iyer, R. K.; Moorthy, P. N. *J. Chem. Soc., Dalton Trans.* **1994**, 3711.
(22) (a) Thomas, F.; Masion, A.; Bottero, J. Y.; Rouiller, J.; Genévrier, F.; Boudot, D. *Environ. Sci. Technol*. **1991**, *25*, 1553. (b) Thomas, F.; Masion, A.; Bottero, J. Y.; Rouiller, J.; Montingy, F.; Genévrier, F. *Environ. Sci. Technol*. **1993**, *27*, 2511.
(23) Faust, B. C.; Labiossa. W. B.; Dai, K. H.; MacFall, J. S.; Browne, B. A.; Ribeiro, A. A.; Richter, D. D. *Geochim. Cosmochim. Acta* **1995**, *59*, 2651.
(24) Tapparo, A.; Heath, S. L.; Jordan, P. A.; Moore, G. R.; Powell, A. K. *J. Chem. Soc., Dalton Trans*. **1996**, 1601.
(25) Kummert, R.; Stumm, W. *J. Colloid Interface Sci*. **1980**, *75*, 373.
(26) Frisch, M. J.; Trucks, G. W.; Schlegel, H. B.; Gill, P. M. W.; Johnson, B. G.; Robb, M. A.; Cheeseman, J. R.; Keith, R.; Petersson, G. A.; Montgomery, J. A.; Raghavachari, K.; Al-Laham, M. A.; Zakrzewski, V. G.; Ortiz, J. V.; Foresman, J. B.; Peng, C. Y.; Ayala, P. Y.; Chen, W.; Wong, M. W.; Andres, J. L.; Replogle, E. S.; Gomperts, R.; Martin, R. L.; Fox, D. J.; Binkley, J. S.; Defrees, D. J.; Baker, J.; Stewart, J. P.; Head-Gordon, M.; Gonzalez, C.; Pople, J. A. *Gaussian 94*, revision C.3; Gaussian, Inc.: Pittsburgh, PA, 1995.
(27) Sykes, D.; Kubicki, J. D.; Farrar, T. C. *J. Phys. Chem. A* **1997**, *101*, 2715.
(28) (a) Kubicki, J. D.; Sykes, D.; Rossman, G. R. *Phys. Chem. Miner*. **1993**, *20*, 425. (b) Kubicki, J. D.; Blake, G. A.; Apitz, S. E. *Geochim. Cosmochim. Acta* **1996**, *60*, 4897.
(29) Sánchez-Marcos, E.; Pappalardo, R. R.; Rinaldi, D. *J. Phys. Chem.* **1991**, *95*, 8928.
(30) Peng, C. Y.; Ayala, P. Y.; Schlegel, H. B.; Frisch, M. J. *J. Comput. Chem*. **1996**, *17*, 49.
(31) Pople, J. A.; Schlegel, H. B.; Krishnan, R.; Defrees, D. J.; Binkley, J. S.; Frisch, M. J.; Whiteside, R. A.; Hout, R. F.; Hehre, W. J. *Int. J. Quantum Chem.: Quantum Chem. Symp*. **1981**, *15*, 269.
(32) Kubicki, J. D.; Blake, G. A.; Apitz, S. E. *Geochim. Cosmochim. Acta* **1997**, *61*, 1031.
(33) Aue, D. *Abstr. Papers Am. Chem. Soc*. **1996**, *211*, 130.
(34) Wong, M. W.; Frisch, M. J.; Wiberg, K. B. *J. Am. Chem. Soc*. **1991**, *113*, 4776.
(35) Parchment, O. G.; Vincent, M. A.; Hillier, I. H. *J. Phys. Chem*. **1996**, *100*, 9689.
(36) Keith, T. A.; Frisch, M. J. *Am. Chem. Soc. Symp. Ser*. **1994**, *569*, 22.
(37) Foresman, J. B.; Frisch, Æ. *Exploring Chemistry with Electronic Structure Methods*; Gaussian, Inc.: Pittsburgh, PA, 1996; p 302.
(38) Wong, M. W.; Wiberg, K. B.; Frisch, M. J. *J. Comput. Chem*. **1995**, *16*, 385.
(39) (a) Stewart, J. J. P. *J. Comput. Chem*. **1989**, *10*, 209. (b) Stewart, J. J. P. *J. Comput. Chem*. **1989**, *10*, 221.
(40) Hawkins, G. D.; Lynch, G. C.; Giesen, D. J.; Rossi, I.; Storer, J. W.; Liotard, D. A.; Cramer, C. J.; Truhlar, D. G. *AMSOL: An SCF program including free energies of solvation and class IV charges*; Quantum Chemistry Program Exchange 606 (based in part on *AMPAC 2.1* by Liotard DA, Healy EF, Ruiz JM, and Dewar MJS and on *GEPOL 12.0* by Silla E, Tunon I, and Pascual-Ahuir JL, 1995).
(41) Marcus, Y. *Chem. Rev.* **1988**, *88*, 1475.
(42) Wiberg, K. B.; Hadad, C. M.; Lepage, T. J.; Breneman, C. M.; Frisch, M. J. *J. Phys. Chem*. **1992**, *96*, 671.
(43) Becke, A. D. *Phys. Rev. A* **1988**, *38*, 3098.
(44) Lee, C.; Yang, W.; Parr, R. G. *Phys. Rev. B* **1988**, *37*, 785.
(45) Tuñón, I.; Silla, E.; Bertrán, J. *J. Phys. Chem*. **1993**, *97*, 5547.
(46) Lim, C.; Bashford, D.; Karplus, M. *J. Phys. Chem*. **1991**, *95*, 5610.
(47) Coe, J. V. *Chem. Phys. Lett.* **1994**, *229*, 161.
(48) Wesolowski, D. J.; Palmer, D. A. *Geochim. Cosmochim. Acta* **1994**, *58*, 2947.
(49) Palmer, D. A.; Wesolowski, D. J. *Geochim. Cosmochim. Acta* **1993**, *57*, 2929.
(50) Rashin, A. A.; Honig, B. *J. Phys. Chem*. **1985**, *89*, 5588.
(51) Palmer, D. A.; Bell, J. L. S. *Geochim. Cosmochim. Acta* **1994**, *58*, 651.
(52) Rosseinsky, D. R. *Chem. Rev.* **1965**, *65*, 467.
(53) Ridley, M. K.; Palmer, D. A.; Wesolowski, D. J.; Kettler, R. M. *Geochim. Cosmochim. Acta* **1998**, *62*, 2279.
(54) Akitt, J. W.; Mann, B. E. *J. Magn. Reson*. **1981**, *44*, 584.
(55) Tossell, J. A. *Magn. Reson*., in press.
(56) Öhman, L.-O. *Acta Chem. Scand*. **1991**, *45*, 258.
(57) Yang, M. M.; Crerar, D. A.; Irish, D. E. *Geochim. Cosmochim. Acta* **1989**, *53*, 319.
(58) Bombi, G. G.; Corrain, G.; Sheikh-Osman, A. A.; Valle, G. *Inorg. Chim. Acta* **1990**, *171*, 79.
(59) Perdew, J. P.; Wang, Y. *Phys. Rev. B* **1991**, *45*, 13244.
(60) Mhatre, S. N.; Iyer, R. K.; Moorthy, P. N. *Magn. Reson. Chem*. **1993**, *31*, 169.
(61) Golic, L.; Leban, I.; Bulc, N. *Acta Crystallogr*. **1989**, *45*, 44.
(62) Phillips, B. L.; Crawford, S. N.; Casey, W. H. *Geochim. Cosmochim. Acta* **1997**, *61*, 4965.
(63) Venema, F. R.; Peters, J. A.; van Bekkum, H. *J. Chem. Soc., Dalton Trans*. **1990**, 2137.
(64) Jaber, M.; Bertin, F.; Thomas-David, G. *Can. J. Chem*. **1977**, *55*, 3689.
(65) Feng, T. L.; Gurian, P. L.; Healy, D.; Barron, A. R. *Inorg. Chem*. **1990**, *29*, 408.
(66) Powell, A. K.; Heath, S. L. *Coord. Chem. Rev*. **1996**, *149*, 59.
(67) Biber, M. V.; Stumm, W. *Environ. Sci. Technol*. **1994**, *28*, 764.
(68) Bottero, J. Y.; Cases, J. M.; Fiessinger, F.; Poirier, J. E. *J. Phys. Chem*. **1980**, *84*, 2933.
(69) Shock, E. L.; Koretsky, C. M. *Geochim. Cosmochim. Acta* **1993**, *57*, 4899.
(70) Dowty, E. *ATOMS for Windows*, v3.1; Shape Software: Kingsport, TN, 1995.